^{13}C, ^{18}O, and D Fractionation Effects in the Reactions of CH_3OH Isotopologues with Cl and OH Radicals

Karen L. Feilberg,[†] Margret Gruber-Stadler,[‡,§] Matthew S. Johnson,[†] Max Mühlhäuser,[§] and Claus J. Nielsen*[,‡]

Department of Chemistry, University of Copenhagen, Universitetsparken 5, DK-2100 Copenhagen OE, Denmark, Centre for Theoretical and Computational Chemistry, Department of Chemistry, University of Oslo, Pb. 1033 - Blindern, N-0315 Oslo, Norway, and Studiengang Umwelt-, Verfahrens- & Biotechnik, MCI - Management Center Innsbruck Internationale Fachhochschulgesellschaft mbH, Egger-Lienz-Straβe 120, A-6020 Innsbruck, Austria

Received: June 26, 2008; Revised Manuscript Received: August 26, 2008

A relative rate experiment is carried out for six isotopologues of methanol and their reactions with OH and Cl radicals. The reaction rates of CH_2DOH, CHD_2OH, CD_3OH, $^{13}CH_3OH$, and $CH_3{}^{18}OH$ with Cl and OH radicals are measured by long-path FTIR spectroscopy relative to CH_3OH at 298 ± 2 K and 1013 ± 10 mbar. The OH source in the reaction chamber is photolysis of ozone to produce $O(^1D)$ in the presence of a large excess of molecular hydrogen: $O(^1D) + H_2 \rightarrow OH + H$. Cl is produced by the photolysis of Cl_2. The FTIR spectra are fitted using a nonlinear least-squares spectral fitting method with measured high-resolution infrared spectra as references. The relative reaction rates defined as $\alpha = k_{light}/k_{heavy}$ are determined to be: $k_{OH + CH_3OH}/k_{OH + {}^{13}CH_3OH} = 1.031 \pm 0.020$, $k_{OH + CH_3OH}/k_{OH + CH_3{}^{18}OH} = 1.017 \pm 0.012$, $k_{OH + CH_3OH}/k_{OH + CH_2DOH} = 1.119 \pm 0.045$, $k_{OH + CH_3OH}/k_{OH + CHD_2OH} = 1.326 \pm 0.021$ and $k_{OH + CH_3OH}/k_{OH + CD_3OH} = 2.566 \pm 0.042$, $k_{Cl + CH_3OH}/k_{Cl + {}^{13}CH_3OH} = 1.055 \pm 0.016$, $k_{Cl + CH_3OH}/k_{Cl + CH_3{}^{18}OH} = 1.025 \pm 0.022$, $k_{Cl + CH_3OH}/k_{Cl + CH_2DOH} = 1.162 \pm 0.022$ and $k_{Cl + CH_3OH}/k_{Cl + CHD_2OH} = 1.536 \pm 0.060$, and $k_{Cl + CH_3OH}/k_{Cl + CD_3OH} = 3.011 \pm 0.059$. The errors represent 2σ from the statistical analyses and do not include possible systematic errors. Ground-state potential energy hypersurfaces of the reactions were investigated in quantum chemistry calculations at the CCSD(T) level of theory with an extrapolated basis set. The ^2H, ^{13}C, and ^{18}O kinetic isotope effects of the OH and Cl reactions with CH_3OH were further investigated using canonical variational transition state theory with small curvature tunneling and compared to experimental measurements as well as to those observed in CH_4 and several other substituted methane species.

1. Introduction

Methanol is one of the most abundant oxygenated hydrocarbons in the troposphere and constitutes a significant fraction of the total nonmethane hydrocarbon (NMHC) burden in the atmosphere with average concentrations second only to methane. Tropospheric boundary layer concentrations of methanol exhibit large spatial variations and are typically ~900 pptv over the remote ocean and ~2000 pptv in remote continental regions; however, they can reach 20 ppb in forested and urban areas.[1] Although published budgets vary, all agree that at least 60% of the global methanol source is from the terrestial biosphere including plant emissions. Methanol is produced for example by pectin demethylation in expanding foliage.[2] There are significant uncertainties in the known sources and sinks of methanol.[3] There are few measurements of methanol concentrations in the field, and recent evaluations of the total source suggest unknown sinks must exist.[4,5] Methanol is itself a significant sink for OH radicals in the gas phase, and its oxidation is a source of HCHO, HO_2, and indirectly O_3. As it is soluble in water, methanol oxidation to HCHO and HCOOH in the liquid phase can alter the oxidative capacity and acidity of cloud droplets.[6] Heterogeneous reactions on droplets have also been suggested for CH_3OH, but these are not fully understood.[5] In coastal areas and in the marine boundary layer, the reaction of CH_3OH with atomic chlorine is likely to contribute to removal, as it does for methane.[7] The anthropogenic source of CH_3OH is minor, but it is likely to increase in the future as plant derived methanol is coming into use as an alternative combustion engine fuel.

The photochemical source of methanol is the reaction of methylperoxy radicals with peroxyradicals—mainly other methyl peroxyradicals from the oxidation of methane but NMHCs also contribute. This source is difficult to quantify as the RO_2 radicals can undergo several different reactions. The reactions that lead to the formation of methanol from methane include

$$CH_4 + OH \rightarrow CH_3 + H_2O \quad (1)$$

$$CH_3 + O_2 + M \rightarrow CH_3O_2 + M \quad (2)$$

$$CH_3O_2 + HO_2 \rightarrow CH_3OOH + O_2 \quad (3)$$

$$CH_3O_2 + NO \rightarrow CH_3O + NO_2 \quad (4)$$

$$CH_3O_2 + CH_3O_2 \rightarrow CH_3O + CH_3O + O_2 \quad (5a)$$

$$CH_3O_2 + CH_3O_2 \rightarrow HCHO + CH_3OH + O_2 \quad (5b)$$

$$CH_3O + O_2 \rightarrow HCHO + HO_2 \quad (6)$$

In high NO_x conditions, reaction 4 will remove most of the RO_2 radicals, but in the remote atmosphere, a significant amount, $k_{5b}/(k_{5a} + k_{5b}) = 0.41$,[8] will self-react via 5b leading to CH_3OH formation.

* Corresponding author. E-mail: c.j.nielsen@kjemi.uio.no.
† University of Copenhagen.
‡ University of Oslo.
§ Management Center Innsbruck Internationale Fachhochschulgesellschaft mbH.

10.1021/jp805643x CCC: $40.75
Published on Web 10/09/2008

A possible method for tracing methanol originating from methane oxidation is to study the isotopic composition of CH_4 and CH_3OH measured in the atmosphere knowing the kinetic isotope effects in the reactions that convert CH_4 to methanol and other products. The study of isotopic fractionation has proven to be a useful tool for tracing sources and sinks of several atmospheric trace components.[9] The isotopic composition of CH_4 can distinguish fossil fuel sources from agricultural sources,[10] and the ^{13}C and D kinetic isotope effects in the reactions of CH_4 with OH, Cl, and $O(^1D)$ can be used to constrain the methane budget.[11] The isotopic composition of CO is known to be shifted by reaction with OH, and studies of the ^{18}O and ^{17}O enrichment can give knowledge of the photochemical history of the CO, as well as provide a proxy for OH radicals.[12] Isotope effects in atmospheric photolysis have likewise been employed for tracing atmospheric trace gases, such as OCS, N_2O, and CO_2.[13−15] Photolysis of formaldehyde is the largest single source of atmospheric H_2, and the isotope effect in the photolysis of HCHO vs HCDO can be used to constrain the budget of H_2.[16,17]

Knowledge of the isotope effects in the processes throughout the oxidation chain from methane (and hydrocarbons in general) to CO_2 can be used to trace the flow of material originating in CH_4, and at later stages the ^{17}O and ^{18}O signatures, through to stable products further down the chain, thus constraining the budgets of CH_4, HCOOH, CH_3OH, HCHO, CO, CO_2, and H_2. Characterization of the kinetic isotope effects in the reactions of methanol isotopologues with OH and Cl radicals may provide additional information about the atmosphere not available from other sources.[9] Hydrogen abstraction from methane and substituted methanes are some of the most intensively studied systems in theoretical chemistry, and the kinetic isotope effects (KIEs) can provide important information about the potential energy surfaces of these reactions. The present study presents results for the reaction rates of CH_2DOH, CHD_2OH, CD_3OH, $^{13}CH_3OH$, and $CH_3{}^{18}OH$ with Cl and OH radicals measured relative to CH_3OH. There are three previous experimental studies of kinetic isotope effects available. Hess and Tully[18] measured the absolute rate coefficients for the reactions of OH with CH_3OH and CD_3OH over the temperature range of 293−866 K using the laser photolysis/laser-induced fluorescence technique and determined the KIE to yield insight into the branching ratio for H-atom abstraction from the methyl versus the hydroxyl site in methanol. McCaulley et al.[19] performed kinetic studies for seven isotopic variants of the $OH + CH_3OH$ reaction at room temperature and 3 Torr pressure using a discharge flow reactor with laser-excited fluorescence detection of OH and OD. Greenhill and O′Grady[20] determined the rate coefficients of the hydroxyl reaction with methanol in the temperature range of 260−803 K as well as with methanol-1,1,1-d_3 at 293 K by flash photolysis combined with resonance absorption detection of OH. To elucidate the mechanism behind the observed kinetic isotope effects, we performed quantum chemistry calculations to model the reactions using variational transition state theory (VTST). None of the previous theoretical studies of the Cl reaction with methanol[21−27] have considered the kinetic isotope effects. Only one[28] of many theoretical studies[29−34] of the OH reaction with methanol investigated the kinetic and geometrical isotope effects in the hydrogen transfer reactions.

2. Experimental and Computational Methods

2.1. Relative Rate Exeriments. The kinetic study was carried out using the relative rate method in a static gas mixture, in which the decays in the concentrations of the reacting species were measured simultaneously as a function of reaction time. This well-established method has been described in detail elsewhere,[35] and a brief description follows here.

Consider two simultaneous bimolecular reactions with the rate coefficients k_A and k_B

$$A + X \xrightarrow{k_A} \text{products} \qquad B + X \xrightarrow{k_B} \text{products} \tag{7}$$

Assuming that there are no other loss processes than these reactions and that there is no production of A and B, then the following relation is valid

$$\ln\left\{\frac{[A]_0}{[A]_t}\right\} = \frac{k_A}{k_B}\ln\left\{\frac{[B]_0}{[B]_t}\right\} \tag{8}$$

where $[A]_0$, $[A]_t$, $[B]_0$, and $[B]_t$ denote the concentrations of the compounds A and B at times zero and t, respectively. A plot of $\ln([A]_0/[A]_t)$ vs $\ln([B]_0/[B]_t)$ will thus give the relative reaction rate coefficient $\alpha = k_A/k_B$ as the slope, or in terms of the fractionation constant, $\varepsilon = \alpha - 1$. In these experiments, A is $^{12}CH_3{}^{16}OH$, and B represents the heavier ^{13}C, D, and ^{18}O substituted isotopologues.

The experiments were carried out in a 250 L electropolished stainless steel smog chamber equipped with a White-type multiple reflection mirror system with a 120 m optical path length for FTIR detection. All experiments were carried out in synthetic air (AGA, 99.99% purity; 4:1 N_2:O_2; CO, NO_x, and C_nH_m less than 1 ppm) at 298 ± 2 K and 1013 ± 10 mbar. Each heavy isotopologue was studied individually with CH_3OH, and each experiment was carried out at least twice.

The infrared spectra were recorded with Bruker IFS 88 and IFS 66v FTIR instruments equipped with liquid nitrogen cooled InSb detectors and an 1800−4000 cm^{-1} band-pass filter. A total of 128 scans were coadded, each with a nominal resolution of 0.125 cm^{-1} (OPD = 8 cm) and using boxcar apodization. Infrared spectra were recorded at regular intervals during ca. 1.5 h to monitor the relative decay of the methanol isotopologues. The standard experiments consisted of 8−12 steps of 1−2 min photolysis for Cl and 3−5 min photolysis for OH followed by a 1 min waiting period and 2 min of data collection with the lamps turned off. The experiments were stopped when about 1/3 of the CH_3OH initially present had been consumed.

Control experiments were performed to check for loss of methanol via photolysis, dark chemistry, and heterogeneous reactions in the reactor. The lifetime of methanol in the reaction chamber was investigated with purified air as diluent and with the relevant radical precursor mixtures included in experiments lasting from 5 to 7 h. The photo stability of methanol toward the radiation used in generating the radicals was studied in a separate experiment with purified air as diluent: no direct photolysis in the reactor was detected.

The experimental spectra were analyzed using a nonlinear least-squares spectral fitting procedure, developed by D. W. T. Griffith.[36,37] In this method, the spectrum of the mixture of absorbing species is first simulated by calculation from initial estimates of the absorber concentrations.[38] The calculation is then iterated to minimize the residual between the measured and simulated spectrum. In the spectrum calculation, true absorption coefficients are normally calculated from HITRAN line parameter data, and the transmission spectrum is computed and then convolved with the FTIR instrument function to simulate the measured spectra. If HITRAN line parameter data are not available, a scaled quantitative laboratory spectrum

measured at high resolution can be used as a good approximation to the absorption coefficients. The iterative fitting follows the Levenberg−Marquardt algorithm to adjust the calculation parameters (absorber concentrations, continuum level, and instrument line shape parameters) and achieves a least-squares minimum residual between measured and simulated spectra in typically 5−10 iterations. Examples of spectral fits are shown in Figure 1 including the residuals of the fits.

The spectral features used in the analyses were the C−H stretching bands of CH_3OH, CH_2DOH, CHD_2OH, $^{13}CH_3OH$, and $CH_3{}^{18}OH$ in the 2800−3200 cm^{-1} region and the C−D stretching band of CD_3OH in the 2000−2200 cm^{-1} region. For the methanol isotopologues, experimental high-resolution IR spectra were used as spectral data in the least-squares algorithm. High-resolution spectra of HCDO and DCDO were also used in the fits, and spectral data for all other components observed in the spectra were taken from the HITRAN database: HCHO, CH_4, H_2O, HDO, O_3, CO, N_2O, and CO_2.[39]

2.2. Materials. The CH_3OH used was standard spectroscopic grade (≥99%) from Sigma-Aldrich and was purified by several freeze−pump−thaw cycles prior to use. CH_2DOH (98%), CHD_2OH (98%), CD_3OH (99%), and $^{13}CH_3OH$ (99%) were purchased from Cambridge Isotopes and used without further purification. $CH_3{}^{18}OH$ was purchased from Campro Scientific (99%). Hydroxyl radicals were generated by photolysis of O_3 in the presence of a large excess of H_2. The volume fractions of H_2 (AGA 4.5) and ozone were around 3×10^3 ppm and 400 ppm, respectively, and the volume fraction of each CH_3OH isotopologue was 3 ppm. Ozone was produced from O_2 (AGA 4.5) by using a MK II Ozone generator from BOC that converts approximately 5% of the oxygen gas flow to ozone. The ozonizer occasionally produced N_2O in the discharge; however, this was easily accounted for in the analysis.

$$O_3 + h\nu(\lambda \sim 254\ \text{nm}) \rightarrow O(^1D) + O_2 \quad (9)$$

$$O(^1D) + H_2 \rightarrow OH + H \quad (10)$$

$$O(^1D) + M \rightarrow O(^3P) + M \quad (11)$$

$$H + O_3 \rightarrow OH + O_2 \quad (12)$$

$$H + O_2 + M \rightarrow HO_2 + M \quad (13)$$

$$HO_2 + O_3 \rightarrow OH + 2O_2 \quad (14)$$

Reaction 10 leads to the formation of OH radicals in both the vibrational ground-state and vibrationally excited states.[40−42] Literature values for the collisional quenching rates of vibrationally excited OH by O_2 and N_2 are of the order of 10^{-15} and 10^{-13} cm^3 $molecule^{-1}$ s^{-1}, respectively,[43] which is comparable to the OH reaction rate with CH_3OH. However, the concentrations of O_2 and N_2 are a factor 10^5 higher than the CH_3OH concentration. It can therefore be assumed that CH_3OH almost exclusively reacts with OH in the vibrational ground state.

The chlorine atoms were generated by photolysis of Cl_2 using Philips TLD-08 fluorescence lamps ($\lambda_{max} \sim 350$ nm) leading to the production of ground-state chlorine atoms. Cl_2 (20 ppm standard laboratory grade) was introduced to the chamber after purification by several freeze−pump−thaw cycles.

$$Cl_2 + h\nu(\lambda \sim 350\ \text{nm}) \rightarrow 2Cl(^2P_{3/2}\ \text{exclusively}) \quad (15)$$

The CH_3OH isotopologues and the Cl_2 or H_2 gas were flushed into the reaction chamber with synthetic air via a Pyrex gas handling system. Ozone was introduced via a Teflon tube from the ozonizer, and the chamber was subsequently filled to 1013 mbar. The pressures of the reactants were measured in a standard volume on the gas line by a 10 mbar range capacitance manometer. Prior to experiments, the chamber was passivated by photolyzing O_3 to eliminate impurities in the system.

2.3. Electronic Structure Calculation. MP2[44] and CCSD(T)[45] calculations were carried out with the Gaussian 03 program.[46] Unrestricted wave functions were used to describe open shell systems and bond breaking processes; singlet ground-state structures were calculated using a restricted wave function. The core electrons were kept frozen in the calculations. Dunning's correlation-consistent aug-cc-pVXZ (X = D, T, and Q) basis sets[47,48] were employed in all calculations. CCSD(T)/aug-cc-pVXZ (X = D, T, and Q) single-point correlation energies were extrapolated toward the basis-set limit using the extrapolation scheme of Halkier et al.[49]

$$E_{XY}^{\infty} = \frac{X^3 E_X - Y^3 E_Y}{X^3 - Y^3} \quad (16)$$

where E_X is the correlation energy obtained with the highest cardinal number X, and E_Y is the correlation energy obtained

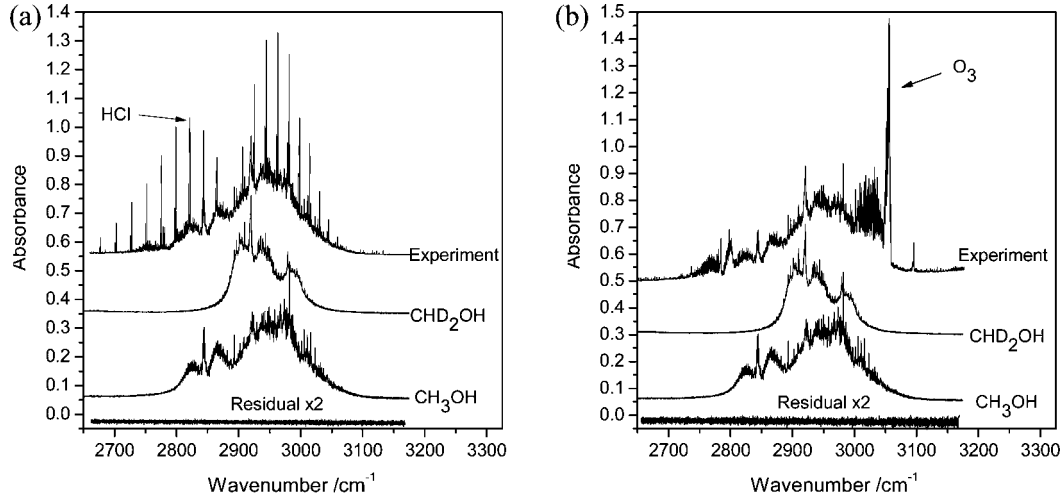

Figure 1. (a) Experimental spectrum of a mixture of CH_3OH and CHD_2OH in the C−H stretching region, 2800−3200 cm^{-1}, for a Cl radical experiment. The υ_1 band of HCl overlaps the CH_3OH bands. (b) An experimental spectrum of a mixture of CH_3OH and CHD_2OH in the CH stretching region, 2800−3200 cm^{-1}, for an OH radical experiment. The 3 υ_3 band of O_3 is seen in the spectrum as well as the C−H stretching bands of HCHO and HCDO. The residuals of the fits and the high-resolution spectra of both isotopologues used to fit the spectrum are shown beneath the experimental spectra.

with cardinal number Y equal to $X - 1$. The cardinal numbers of the aug-cc-pVXZ (X = D, T, Q) basis sets are 2, 3, and 4, respectively. In the following, such calculations will be denoted CCSD(T)/EB$_{XY}$ with "EB" being short for extrapolated basis.

The minimum energy path (MEP) connecting reactants and products was computed at the MP2/aug-cc-pVTZ level of theory using the intrinsic reaction coordinate (IRC) method of Gonzales and Schlegel.[50,51] The IRC calculations were carried out in mass-weighted Cartesian coordinates using a step size of 0.02 u$^{1/2}$ bohr.

2.4. Calculations of Rate Coefficients. Calculations of rate coefficients were carried out using interpolated variational transition state theory by mapping (IVTST-M)[52] using the sparse grid of geometries, gradients, and Hessians from the ab initio IRC calculations as input. The MEP was followed in mass-scaled (scaling mass equal to 1 u) curvilinear coordinates using the RODS algorithm.[53] In all reactions, a step size of 0.003 bohr was used. The electronic energy of the MEP was corrected by the interpolated single-point energy method (ISPE)[54] using the extrapolated CCSD(T) energies computed at all stationary points as input. From this information, the ground-state vibrationally adiabatic potential curve, ΔV_a^G, was obtained.

The POLYRATE program[55] was used to calculate the rate coefficients over the temperature range of 200−1500 K using improved canonical variational theory (ICVT)[56,57] for the chlorine reactions and canonical variational theory (CVT)[57,58] for the OH reactions. Semiclassical tunneling corrections have been included using the centrifugal-dominant small-curvature adiabatic ground-state tunneling (called small-curvature tunneling or SCT) approximation.[57,59] The transmission coefficient also includes the classical adiabatic ground-state (CAG) transmission coefficient[60] that adjusts the quantal corrections for the difference between V_a^G at its maximum and at the CVT transition state. The calculation of the kinetic isotope effects were based on a single reaction path using the methods outlined in refs 53, 61, and 62.

In the chlorine reaction, the two spin−orbit states $^2P_{3/2}$ (lowest) and $^2P_{1/2}$ of Cl having degeneracies of 4 and 2, respectively, and separated by 882 cm^{-1} were included in the calculation of the electronic partition function. Similarly, in the OH reaction, the $^2\Pi_{3/2}$ and $^2\Pi_{1/2}$ states of the OH radical were included, both having degeneracy equal to 2 and separated by 140 cm^{-1}. To estimate the contribution of SO coupling to the potential energy surfaces of reactions, SO matrix elements were calculated for the stationary points obtained at the MP2/aug-cc-pVTZ level of theory using the Breit−Pauli Hamiltonian as implemented in the Molpro 2002.6 program package.[63,64] Wave functions for the SO states were generated using MRCI with reference CASSCF configurations only and the 6-311++G(3df, p) basis set.

The vibrational−rotational partition functions were assumed to be separable, and the rotational partition functions were approximated by their classical limit. The vibrational partition functions were calculated within the harmonic oscillator approximation for all modes, except the C···H···OH torsional mode in the transition states of the CH_3OH + OH reactions which were handled by the hindered rotor RWO scheme.[65−67] The potentials of the torsional modes, $V(\phi)$, were calculated at the MP2/aug-cc-pVTZ level of theory and fitted to $V_j(\phi) = U_j + 1/2W_j[1 - \cos 2(\phi-\phi_j)]$, where U_1 is 0, U_j is the height of each distinct potential minimum relative to the lowest one, and W_j is a symmetric approximation to the barrier to internal rotation away from the minimum at $\phi = \phi_j$. For the C−H abstraction reaction, two distinct barriers with heights of W_1 = 499 cm^{-1} and W_2 = 301 cm^{-1} separated by a shallow minimum of U_2 = 295 cm^{-1} were found. For the O−H abstraction reaction, two barriers with heights of W_1 = 857 cm^{-1} and W_2 = 815 cm^{-1} with a minimum of U_2 = 2 cm^{-1} were found.

3. Results and Discussion

3.1. Experimental Study. The chemistry in the reaction chamber is as follows (rate constants in units of cm^3 molecule^{-1} s^{-1})[68,69]

$$CH_3OH + OH \rightarrow CH_2OH/CH_3O + H_2O \qquad k_{298} = 9.0\times10^{-13} \quad (17)$$

$$CH_3OH + Cl \rightarrow CH_2OH + HCl \qquad k_{298} = 5.5\times10^{-11} \quad (18)$$

$$CH_3OH + O(^3P) \rightarrow CH_2OH/CH_3O + OH \qquad k_{298} = 7.5\times10^{-15} \quad (19)$$

$$CH_3O + O_2 \rightarrow HCHO + HO_2 \qquad k_{298} = 1.9\times10^{-15} \quad (6)$$

$$CH_2OH + O_2 \rightarrow HCHO + HO_2 \qquad k_{298} = 9.7\times10^{-12} \quad (20)$$

$$HCHO + h\nu \rightarrow HCO + H;\ H_2 + CO \quad \text{(OH exp. only)} \quad (21)$$

$$HCHO + OH/Cl + O_2 \rightarrow HO_2 + CO + H_2O/HCl \Rightarrow CO_2 \quad (22)$$

In the OH experiments, O(^{3}P) is generated from O(^{1}D) and the thermal decomposition of O_3. O(^{3}P) reacts with CH_3OH via reaction 19, and a small amount of CO was observed when CH_3OH and O_3 were left in the dark in the cell for 2 h. To test the extent of this problem, a model of the reaction system was constructed using the FACSIMILE software package.[70] Fifty-one reactions were included with kinetic data from the NIST database[71] and the JPL evaluation,[72] and the result is shown in Figure S1 (Supporting Information). The O(^{3}P) contribution in the modeled experiment amounts to less than 0.5% of the total methanol loss, and it can therefore be regarded as negligible. The model also shows that HO_2 formed in reactions 6, 13, and 20 do not present any significant sink for methanol in the reaction chamber. CH_3OOH was not observed in the spectra as it reacts rapidly with the radicals present to form CO and CO_2.

The results of the relative rate studies of the kinetic isotope effects in reactions 17 and 18 are shown in Table 1. The agreement between individual experiments is good which is also reflected in the small error on the weighted average values. The relative rate plots, $\ln([A]_0/[A]_t)$ vs $\ln([B]_0/[B]_t)$, for the five heavy isotopologues, are shown in Figures 2a−2f. A comparison of the d3 KIE in the OH reaction with previous experimental measurements shows that our value of $k_{OH + CH_3OH}/k_{OH + CD_3OH} = 2.566 \pm 0.042$ is somewhat higher than the value of 2.15 ± 0.13 obtained by Hess and Tully[18] and the value of 1.65 measured by Greenhill and O'Grady[20] but lower compared to the value of 3.35 ± 0.72 reported by McCaulley et al.[19]

Methanol is not only removed from the gas phase by radical reactions but also by physisorption/chemisorption on the reactor walls. This "natural" or "dark" removal of CH_3OH from the gas phase (purified air) in the reactor is shown in Figure 3. Assuming the (small) decay to be of first order in CH_3OH, the natural loss rate coefficient was determined to be 1.3×10^{-6} s^{-1}, which corresponds to a lifetime of around 9 days in the chamber. For a realistic reaction mixture in the OH radical experiments ($CH_3OH/H_2/O_3$ = 5:2000:600 ppm in 1013 hPa purified air), the loss rate coefficient of CH_3OH increases to 3×10^{-5} s^{-1} (Figure 3). The methanol loss was observed to be

TABLE 1: Summary of Results[a]

	Cl reaction		ε (%)	OH reaction		ε (%)
isotopologue	no. of exp.	$\alpha = k_{light}/k_{heavy}$	$\varepsilon = (\alpha - 1)$	no. of exp.	$\alpha = k_{light}/k_{heavy}$	$\varepsilon = (\alpha - 1)$
$^{13}CH_3OH$	3	1.055 ± 0.016	55	2	1.031 ± 0.020	31
$CH_3{}^{18}OH$	3	1.025 ± 0.022	25	3	1.017 ± 0.012	16
CH_2DOH	2	1.162 ± 0.022	162	3	1.119 ± 0.045	112
CHD_2OH	2	1.536 ± 0.060	536	5	1.326 ± 0.021	315
CD_3OH	2	3.011 ± 0.059	2011	4	2.566 ± 0.042	1566
$CH_4/^{13}CH_4$		1.058 ± 0.002	58		1.0039 ± 0.0004	3.9
CH_4/CH_3D		1.459 ± 0.006	459		1.294 ± 0.018	294
CH_4/CH_2D_2		2.43 ± 0.01	1430		1.81 ± 0.28	810
CH_4/CHD_3		4.73 ± 0.04	3730		3.30 ± 0.50	2300
CH_4/CD_4		14.7 ± 0.2	13700		7.36 ± 0.88	6360
$CH_3Cl/^{13}CH_3Cl$		1.070 ± 0.010	70		1.059 ± 0.008	59
CH_3Cl/CD_3Cl		4.91 ± 0.07	3910		3.9 ± 0.4	2900

[a] The CH_3OH data are based on the weighted averages of independent experiments. The enrichment factor, ε, is indicated in per mil. Kinetic isotope effects in the reactions of methane and chloromethane with Cl atoms and OH radicals are given for comparison. The CH_4 + Cl reaction data are from Feilberg et al.;[124] the $CH_4/^{13}CH_4$ + OH value is from Saueressig et al;[128] and the remaining CH_4 + OH reaction data are from Gierczak et al.[129] The CH_3Cl data are from Gola et al.[130]

a first-order process with a rate independent of O_3 concentration in the range 200−600 ppm. This is an unusual increase in the removal rate of a compound in our chamber. As the kinetic analysis (eq 8) assumes that only one loss process is taking place, additional loss processes such as gas-phase or surface reactions with the radical precursors and the natural wall loss may give rise to systematic errors in the derived kinetic isotope effects.

The initial OH experiments lasted for 2 1/2−3 h, including the spectral recording time and the waiting time between photolysis, during which around 65% of the initial methanol reacted. This corresponds to a loss rate of around 10^{-4} s^{-1} or only around 3 times that of the "dark" loss rate. The experiments were therefore programmed and carried out as fast as possible by reducing the waiting time between photolysis and recording of spectra to 15 s, by increasing the scanning mirror velocity and by postponing all processing of collected spectra (Fourier transformation of interferograms) such that a complete experiment could be carried out in about 60 min. Under these conditions, the ratio of the methanol loss rates due to reaction with OH radicals and due to the dark reactions is around 10. Taking the rate coefficient for the OH reaction with methanol to be 9.0×10^{-13} cm^3 $molecule^{-1}$ s^{-1},[69] a rough estimate of the average OH concentration during the entire experiment is 3×10^8 molecules cm^{-3}. Assuming that there are no isotope effects in the dark loss processes, a numerical simulation shows that the systematic error in the smallest KIE in the OH radical reactions of 1.017 ± 0.012 (^{18}O) is only −0.001, which can be neglected in comparison to the statistical error in the result. For larger KIEs, the systematic error increases in an exponential manner: for CH_3OH/CH_2DOH, the apparent KIE of 1.119 ± 0.045 may be defective by a systematic error of −0.015; for CH_3OH/CHD_2OH, the apparent KIE of 1.326 ± 0.021 may be off by as much as −0.049. In the worst case, the apparent KIE of 2.566 ± 0.042 for CH_3OH/CD_3OH may have a systematic error amounting to as much as −0.53 without any visible manifestations such as curvature in the relative rate plots. In summary, the known systematic error in the OH radical experiments due to dark reactions of methanol will result in apparent KIEs which are too small. For ^{13}C, ^{18}O, CH_2DOH, and CHD_2OH, the errors are either insignificant or comparable to the 2σ statistical error of the data analyses, but for CD_3OH, the systematic error may be significant. Having made the reservations, we refer to a relative rate study by the Finlayson−Pitts group in which they observed a dark loss of six different alkane blends in air containing ozone or an ozone−water mixture with all the signatures of an OH radical concentration of $\sim 8 \times 10^7$ cm^{-3}.[73] They could essentially reproduce their results using a standard atmospheric chemistry scheme initiated by a slow, perhaps surface-catalyzed, reaction between ozone and the alkane (O_3 + alkane → R + OH + O_2) followed by reactions regenerating the OH radicals with ozone as the driving force. In the present case, the dark loss rate of methanol implies an OH radical concentration of $\sim 3 \times 10^7$ cm^{-3}. To test if this was the case, a few relative rate experiments with $CH_3OH/CD_3OH/O_3/H_2$ mixtures were carried out under dark conditions. The relative rates derived in these experiments varied with the relative amounts of the chemical components, and no firm conclusion could be drawn. We tentatively suggest that part of the enhanced dark loss of methanol in our reaction chamber is due to a similar OH radical generation and that the potential systematic errors in our relative rate results are smaller than indicated above.

The Cl atom experiments generally lasted 2 h and with a methanol conversion of around 65%. The recommended value of the CH_3OH reaction rate coefficient with Cl atoms at 298 K is 5.5×10^{-11} cm^3 $molecule^{-1}$ s^{-1},[69] which places the average Cl atom concentration during the entire experiment around 3×10^6 atoms cm^{-3}. In a typical Cl atom experiment (CH_3OH/Cl_2 = 5:20 ppm in 1013 hPa purified air), the dark loss reaction rate was determined to be 1.4×10^{-6} s^{-1} (Figure 3), which is almost the same as for pure air. This gives a ratio >100 between the loss rates due to Cl atoms and due to the dark processes, and the systematic errors from dark reactions are negligible.

3.2. Structures and Energetics of Stationary Points. Both reactions have theoretically two product channels: in addition to the C−H hydrogen abstraction, the formation of CH_3O radicals via OH hydrogen abstraction is also a possible reaction path:

$$CH_3OH + OH \rightarrow CH_2OH + H_2O \quad (17a)$$

$$CH_3OH + OH \rightarrow CH_3O + H_2O \quad (17b)$$

$$CH_3OH + Cl \rightarrow CH_2OH + HCl \quad (18a)$$

$$CH_3OH + Cl \rightarrow CH_3O + HCl \quad (18b)$$

We have calculated the structures of the stationary points of all four reactions at the MP2/aug-cc-pVXZ (X = D, T, Q) levels of theory. The saddle point structures of the Cl and OH reactions of methanol are displayed in Figure 4. In addition to the saddle point of the hydrogen abstraction reactions, we have located prereaction and postreaction complexes on the MEP for all four reactions. The prereaction adducts are displayed in Figure 5, while the structures of the postreaction adducts can be seen from

Figure 6. The structural results indicate that the aug-cc-pVTZ basis provides a reasonable description of the stationary points. A comparison of the structures obtained with the triple-ζ and quadruple-ζ basis set shows negligible differences in the bond length with the largest deviation of 2.3 pm for the H−Cl bond in the saddle point of the C−H abstraction reaction by chlorine (Figure 4a). When comparing the structural results for CH_3OH with experimental values[74] (Figure S2c, Supporting Information), it is seen that the bond lengths are calculated within a range of less than ± 1.0 pm from the experimental values for the MP2/aug-cc-pVTZ level of theory in agreement with the established error margins.[75] For the CH_2OH and CH_3O radicals, there are no experimental structures available. Theoretical investigations[76−79] predicted that the equilibrium structure of the CH_2OH radical has C_1 symmetry. The symmetry of the minimum energy structure of the CH_3O radical is reduced from C_{3v} to C_s due to Jahn−Teller distortion in the X^2E ground state. As can be seen from Figure S2a and b (Supporting Information), there is an excellent agreement between our calculated equilibrium structures at the MP2/aug-cc-pVXZ (X = T, Q) level

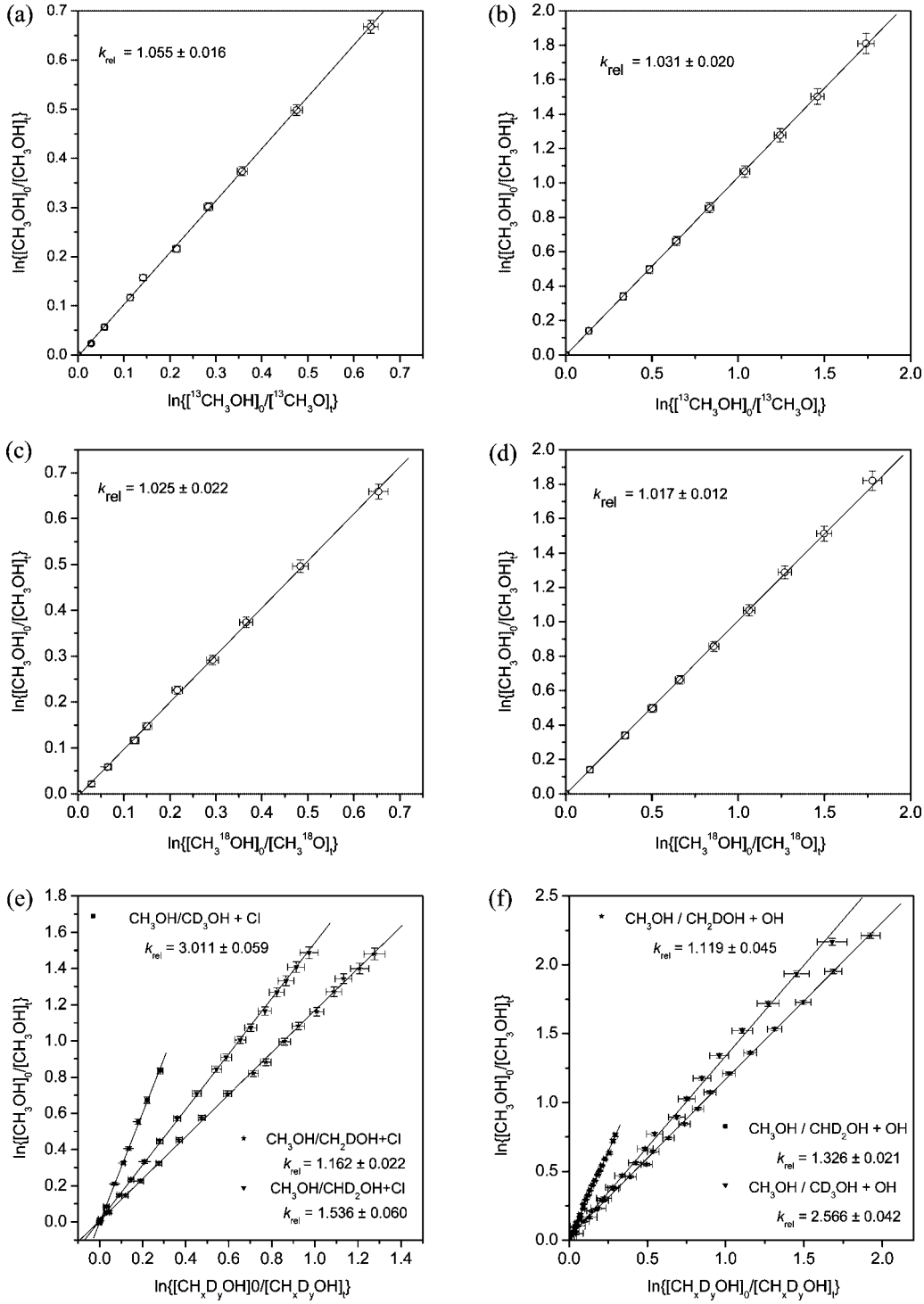

Figure 2. Relative rate plots showing the decays of CH_2DOH, CHD_2OH, CD_3OH, $^{13}CH_3OH$, and $CH_3{}^{18}OH$ relative to CH_3OH for the Cl and OH reactions. The slopes corresponding to the relative reaction rate $\alpha = k_{light}/k_{heavy}$ are given with 2σ errors from the statistical analyses. Figures 2a−2d show the results from a single experiment for $^{13}CH_3OH$ and $CH_3{}^{18}OH$ reacting with Cl and OH, and Figures 2e and 2f show results obtained for CH_2DOH, CHD_2OH, and CD_3OH. The error bars on both axes correspond to 1σ errors.

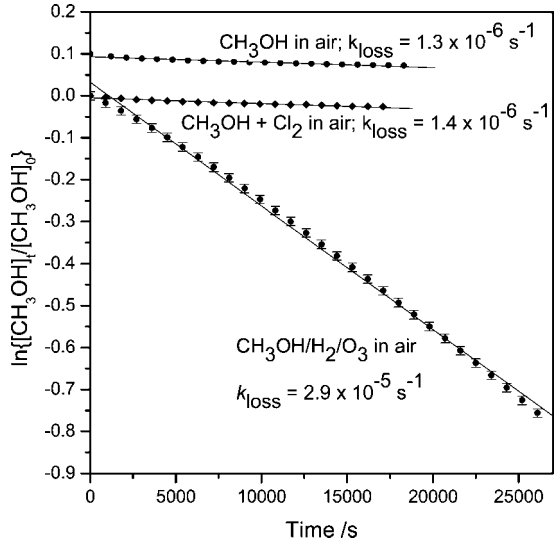

Figure 3. Decay curves for CH_3OH in 1013 hPa purified air in the reactor as a function of time: (a) 5 ppm CH_3OH. (b) 5 ppm CH_3OH/2000 ppm H_2/600 ppm O_3. (c) 5 ppm CH_3OH, 20 ppm Cl_2.

of theory for CH_2OH and CH_3O and those calculated by Marenich and Boggs[79,80] at the CCSD(T)/cc-pVTZ level of theory.

The saddle point structure of the methoxy radical channel of the $CH_3OH + Cl$ reaction in the present study agrees well with that of Jodkowski et al.[22] and Garzón et al.[21] Their saddle point structures as well as the one reported by Rudic et al.[24] and Kollias et al.[26] for the hydroxymethyl radical channel are predicted to be more product-like as compared to our structure. The saddle points for the two channels of the $CH_3OH + OH$ reaction calculated at the PM3[33] and BH&HLYP/6-311G(d,p)[29] levels of theory are also more product-like compared to our structures. Both saddle points reported by Xu et al.[30] and the structure for the methoxy radical channel reported by Jodkowski et al.[31] agree well with our calculations. Again, the structure at the MP2/6-311G** level of theory for the hydroxymethyl radical channel calculated by Jodkowski et al.[31] is predicted to be more product-like than our structure at the MP2/aug-cc-pVTZ level of theory.

We have located postreaction complexes between the hydroxymethyl radical and HCl as well as the methoxy radical and H_2O. The structures depicted in Figures 6a−6c agree reasonably well with the structures reported in previous theoretical studies.[22,23,29−31] Our calculations confirm the existence of a prereaction van der Waals adduct located on the MEP of the $CH_3OH + OH$ reaction for both channels (Figure 5c) which was also reported by Galano et al.[29] and Xu and Lin.[30] Jodkowski et al. did not take this adduct into account in their study.[31] The two different prereaction adducts which we have located on the MEP of the two channels of the $CH_3OH + Cl$ reaction, Figure 5a and 5b, have not been reported previously. Jodkowski et al.[22] and Murray and co-workers[24,27] report in their studies an intermediate molecular complex on the MEP of the $CH_3OH + Cl \rightarrow CH_2OH + HCl$ reaction in which the Cl atom binds to the methanol oxygen. Our IRC calculations, however, in agreement with the findings of Chen and Huang[23] show that this adduct is not located on the MEP of the reaction.

The energetics of the stationary points involved in the reactions are summarized and compared to previous results in Tables S1−S4 (Supporting Information). The agreement with literature data is generally good. The differences between the energies of the CCSD(T) calculations with the largest basis set and the CCSD(T) results with extrapolated basis sets are less than 3 kJ/mol for all reactions indicating that the results are close to the basis set limit of the respective level of theory. In the reaction $CH_3OH + Cl \rightarrow CH_2OH + HCl$, calculations at the CCSD(T) level of theory predict negative Born−Oppenheimer barrier heights (see Table S1, Supporting Information). Taking into account the effect of spin−orbit coupling present in the reaction system, the barrier height is restored to a small, positive value suggesting that the reaction is nearly barrierless. The prereaction adduct is only weakly stabilized by about 6 kJ/mol, and taking into consideration the effects of spin−orbit coupling, the energy is shifted only by +0.3 kJ/mol: spin−orbit coupling is still present in the adduct. Compared to the hydroxymethyl channel, the $CH_3OH + Cl \rightarrow CH_3O + HCl$ reaction is characterized by a much larger Born−Oppenheimer barrier height of 47 kJ/mol at the CCSD(T)/EB_{32}//MP2/aug-cc-pVTZ level of theory (without inclusion of the effect of spin−orbit coupling). The prereaction adduct in this channel is stabilized by 23 kJ/mol, whereas the postreaction adduct is stabilized by 23 kJ/mol relative to the products compared to 16 kJ/mol for the hydroxymethyl channel: all electronic energy values were calculated at the CCSD(T)/EB_{XY}//MP2/aug-cc-pVTZ level of theory.

For the reaction of OH with CH_3OH, the difference between the Born−Oppenheimer barrier heights for the two product channels is smaller than for the Cl reactions: 4.9 versus 15.2 kJ/mol for the CH_2OH and CH_3O channel, respectively, at the CCSD(T)/EB_{32}//MP2/aug-cc-pVTZ level of theory. The adducts in the reaction system are electronically stabilized by 28 kJ/mol (prereaction adduct and postreaction adduct in the CH_2OH channel) and 22 kJ/mol (postreaction adduct in the CH_3O channel). The enthalpies of reaction, $\Delta_{rxn}H°_0$, for the Cl and OH reactions of CH_3OH calculated at the CCSD(T) level of theory with extrapolated basis sets are in reasonable agreement with experimental values with a discrepancy of at most 5 kJ/mol in the CH_3O channel of the OH reaction (Table S1−S4, Supporting Information). For the loosely bound reaction adducts, one might expect the basis set superposition error (BSSE) to be significant. To estimate the magnitude of this effect, the BSSE in the MP2/aug-cc-pVTZ model of the pre- and postreaction adducts for the chlorine and OH reactions of CH_3OH was approximated using the counterpoise correction.[81] The BSSE was found to be between 1.7 (prereaction adducts for the OH reaction and the CH_2OH channel of the Cl reaction) and 7.6 kJ/mol (postreaction adduct of the CH_2OH channel in the Cl reaction).

3.3. Absolute Rate Coefficients. The kinetics of the H-abstraction reactions of CH_3OH with OH (17) and Cl (18) radicals have been extensively studied by theortical[21−26,29−33,82] and experimental[18−21,25,27,83−113] methods. Critical evaluations of the experimental data lead to the currently recommended rate coefficients of $k_{CH_3OH+Cl} = 5.5 \times 10^{-11}$ cm^3 molecule^{-1} s^{-1} independent of temperature over the range 200−580 K[69] and $k(T)_{CH_3OH+OH} = 2.85 \times 10^{-12} \times \exp(-345/T)$ cm^3 molecule^{-1} s^{-1} over the temperature range 210−300 K with $k_{298} = 9.0 \times 10^{-13}$ cm^3 molecule^{-1} s^{-1}.[114] For an extended temperature range of 210−866 K, the three-parameter expression $k(T)_{CH_3OH+OH} = 6.38 \times 10^{-18} \times T^2 \times \exp(144/T)$ cm^3 molecule^{-1} s^{-1} is recommended.[114] Both reactions have a minor product channel in addition to reactions 17a and 18a leading to the formation of CH_3O radicals via reactions 17b and 18b. While reaction 17b has been found to contribute about 5−25% of the total reaction of CH_3OH with OH,[114] the branching ratio of $CH_3OH + Cl$

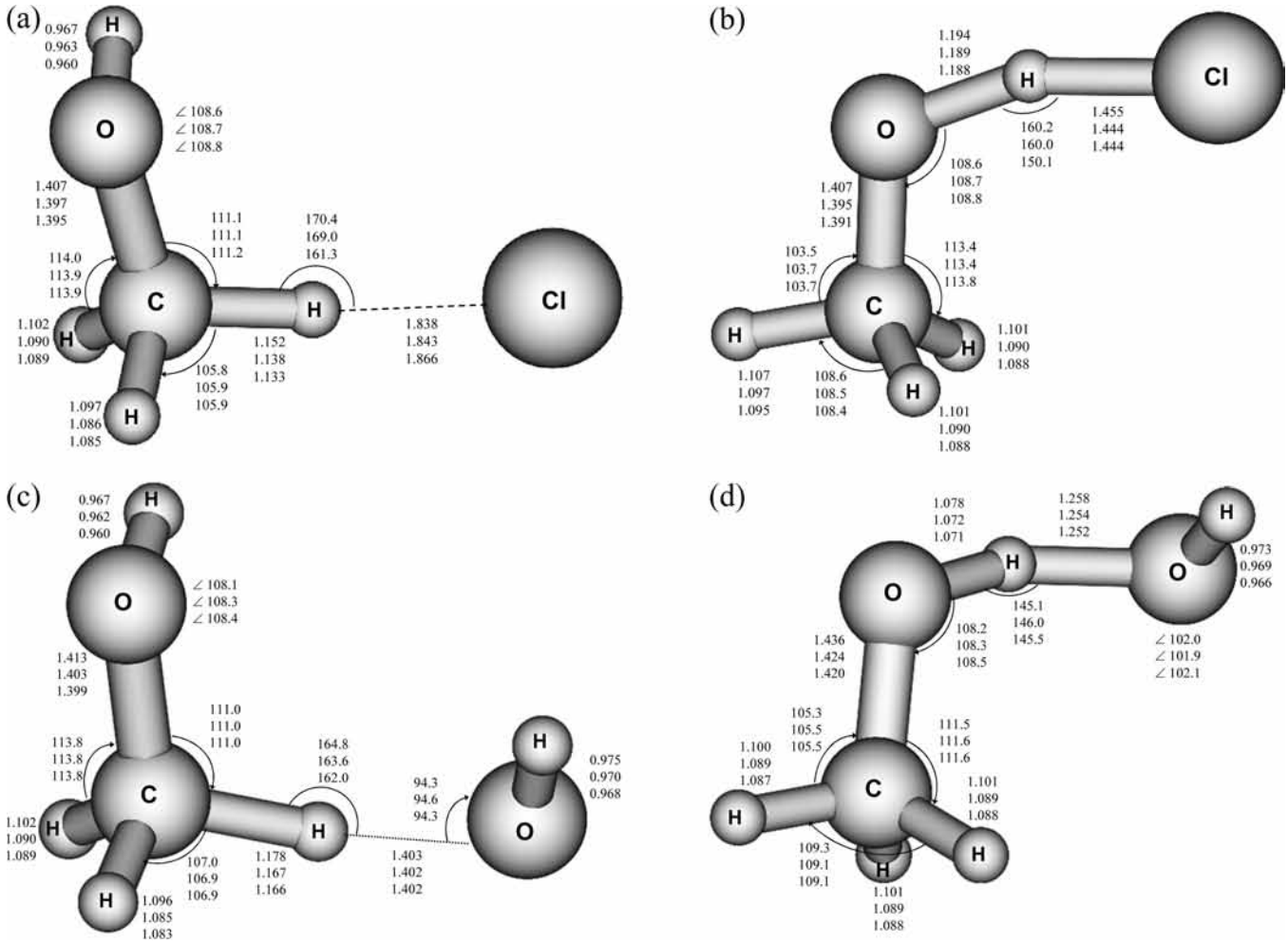

Figure 4. Structures and geometrical parameters of the saddle points of the reactions (a) $CH_3OH + Cl \rightarrow CH_2OH + HCl$, (b) $CH_3OH + Cl \rightarrow CH_3O + HCl$, (c) $CH_3OH + OH \rightarrow CH_2OH + H_2O$, and (d) $CH_3OH + OH \rightarrow CH_3O + H_2O$ calculated at the MP2/aug-cc-pVDZ (top values), MP2/aug-cc-pVTZ, and MP2/aug-cc-pVQZ (bottom values) levels of theory, respectively. Bond lengths are in Angström and bond angles are in degrees.

has been found to be close to 1 and reaction 18b to be almost negligible.[22,87,115]

Figure 7 shows the potential energy of the minimum energy path, V_{MEP}, and the ground-state vibrationally adiabatic potential energy curve, ΔV_a^G, as a function of the reaction coordinate for the $CH_3OH + Cl \rightarrow CH_2OH + HCl$ reaction. The figure also includes the corresponding curves corrected by the ISPE method using single-point energy corrections from CCSD(T)/EB_{43}//MP2/aug-cc-pVTZ calculations. The generalized normal-mode frequencies of the system as a function of the reaction coordinate are shown in Figure S3 (Supporting Information). Figure 8 shows an Arrhenius plot of the calculated rate coefficients for the hydroxymethyl channel of the Cl reaction with methanol. For comparison, the figure includes a plot of the recommended rate coefficient including its uncertainty limits.[69] The effect of spin−orbit coupling originating from the Cl atom becomes smaller during the reaction and will affect the reaction rate by effectively increasing the barrier height. This was taken into account in the calculation of the rate coefficients. On the basis of the MP2/aug-cc-pVTZ MEP, the calculations predicted the SO coupling to lower the asymptotic potential energy of the reactants by 3.3 kJ/mol, in good agreement with the a priori assumption of 1/3 of the SO coupling constant of Cl (3.5 kJ/mol) and previous calculations on similar systems.[116,117] Even so, for the prereaction adduct a spin−orbit coupling of 3.0 kJ/mol was calculated, whereas at the transition state the effect of SO coupling is almost quenched (0.4 kJ/mol). The excited spin−orbit states were only considered in the electronic partition function of the chlorine atom. In the ISPE model, the barrier height was increased by 2.9 kJ/mol according to the SO coupling calculated for the MP2/aug-cc-pVTZ geometries. The reaction enthalpy and the energy of the postreaction adduct were also corrected for the effect of spin−orbit coupling. This method of accounting for SO coupling in dual-level calculations has been shown to give reasonable results for other reaction systems.[117,118] We have also calculated the rate coefficients for the methoxy radical channel, reaction 18b. Figure S4 (Supporting Information) shows an Arrhenius plot of the calculated reaction rates in comparison to the results reported in the theoretical study of Jodkowski et al.[22] The rate coefficients obtained at the ICVT/SCT level applying the ISPE method are more than 4 orders of magnitude lower than the rate coefficients of the hydroxymethyl channel, reaction 18a, at 298 K. Although there is reasonable temperature dependence for the rate coefficients of reaction 18b at 600 K, the reaction rates are still more than 2 orders of magnitude lower than for reaction 18a. Thus, the methoxy radical channel, reaction 18b, is negligible for the reaction of Cl with methanol in agreement with previous experimental[87,89] and theoretical[22] studies which predict a branching ratio for the hydroxymethyl radical channel, reaction 18a, close to unity. The considerable barrier height (27 kJ/mol including ZPE at the CCSD(T)/EB_{32}//MP2/aug-cc-pVTZ

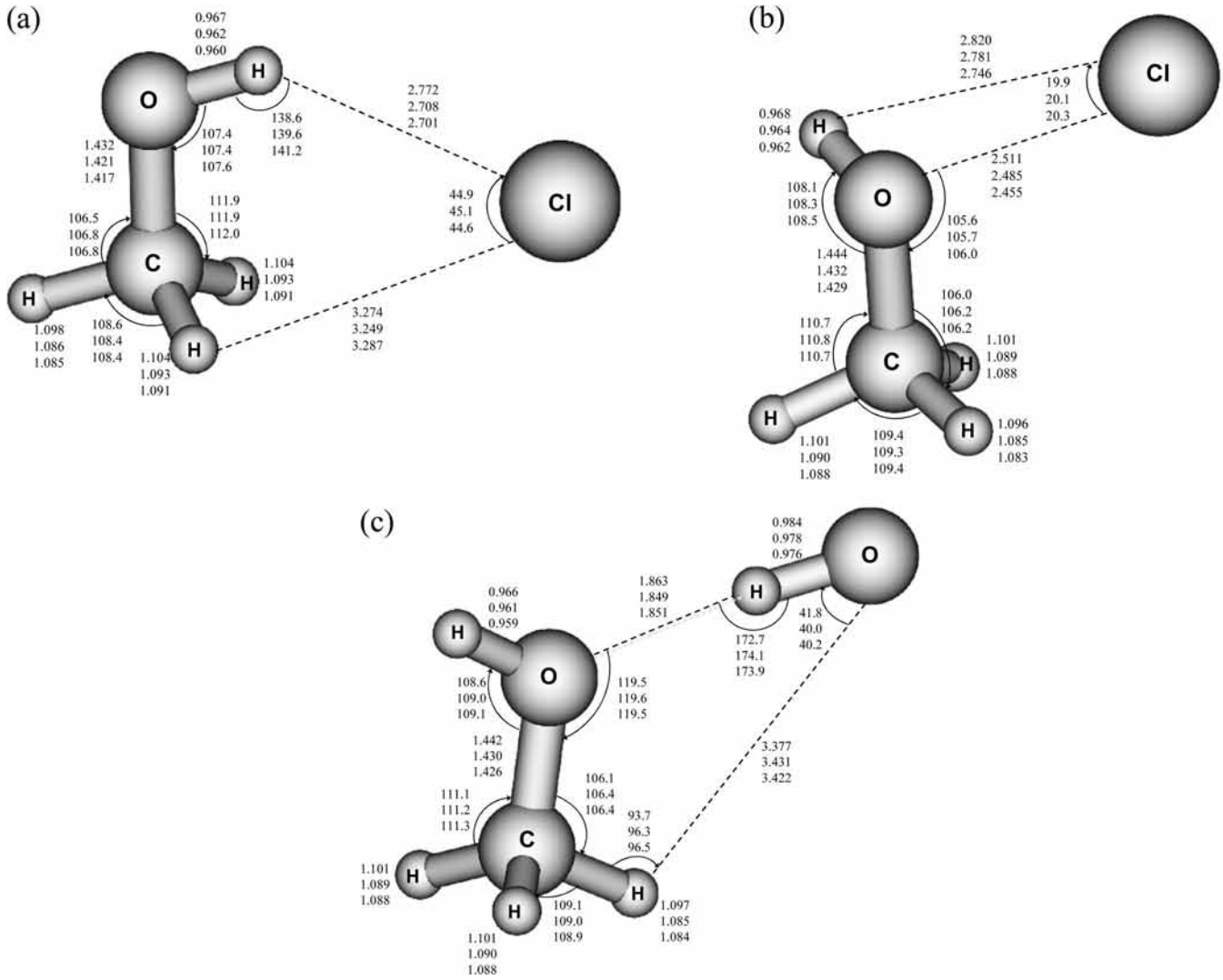

Figure 5. Structures and geometrical parameters of the prereaction van der Waals adducts of the reactions (a) $CH_3OH + Cl \rightarrow CH_2OH + HCl$, (b) $CH_3OH + Cl \rightarrow CH_3O + HCl$, and (c) $CH_3OH + OH \rightarrow CH_2OH + H_2O$; $\rightarrow CH_3O + H_2O$ calculated at the MP2/aug-cc-pVDZ (top values), MP2/aug-cc-pVTZ, and MP2/aug-cc-pVQZ (bottom values) levels of theory, respectively. Bond lengths are in Angström and bond angles are in degrees.

level of theory) and the slight endothermicity of the methoxy channel 18b compared to the almost barrierless exothermic hydroxymethyl channel 18a is in line with the finding that reaction 18a is the main product channel.

We see from Figure 8 that our ICVT/SCT calculations on the MP2/aug-cc-pVTZ PES underestimate the experimental rate coefficient for the $CH_3OH + Cl \rightarrow CH_2OH + HCl$ reaction, whereas applying the ISPE model leads to an overestimation of the recommended experimental reaction rates. The temperature dependence is not correctly reproduced on the MP2 PES: the ISPE model predicts a negative temperature dependence which is considerably pronounced in the low temperature range. The lowering of the barrier height by employing single-point energy corrections at higher levels of theory in the ISPE model increases the rate coefficients significantly compared to the rate coefficients calculated on the MP2/aug-cc-pVTZ PES. Calculations of thermal rate coefficients are, by nature, very sensitive to the precise barrier height of the potential energy surface, in particular for almost barrierless and low-barrier reactions. In the present case, the lowering of the electronic barrier height by only 1.3 kJ/mol in the ISPE model leads to an increase of the rate coefficients by a factor of 2.8 and 2.0 at 200 and 298 K, respectively. The determination of the exact barrier height with an accuracy of 1 kJ/mol is beyond the reach with the methods applied in this study and in general with methods actually available. The second important parameter for the calculation of the rate coefficients is the vibrationally adiabatic potential energy curve, which depends on the vibrational frequencies. We have calculated the vibrational frequencies within the harmonic oscillator approximation. In the present system, however, large anharmonicities can be expected. Studies on the structural and thermochemical properties of CH_3OH,[119] CH_2OH,[76,79] and CH_3O[80,120,121] have shown that couplings of the low-energy frequencies are present in the molecules which cause significant anharmonic behavior in the force fields. These effects can also be expected to play an important role for the complexes involved in the reaction. Thus it would be necessary to take these anharmonicities into account to achieve a more accurate vibrationally adiabatic potential energy curve compared to the applied harmonic approximation.

The V_{MEP} and ΔV_a^G potential energy curves of the OH reaction with CH_3OH at the MP2/aug-cc-pVTZ PES and the corresponding curves corrected by the ISPE-method are given in Figure 9a for the hydroxymethyl channel, reaction 17a, and Figure 9b for the methoxy channel, reaction 17b. The Arrhenius plot of the calculated overall rate coefficients in comparison to

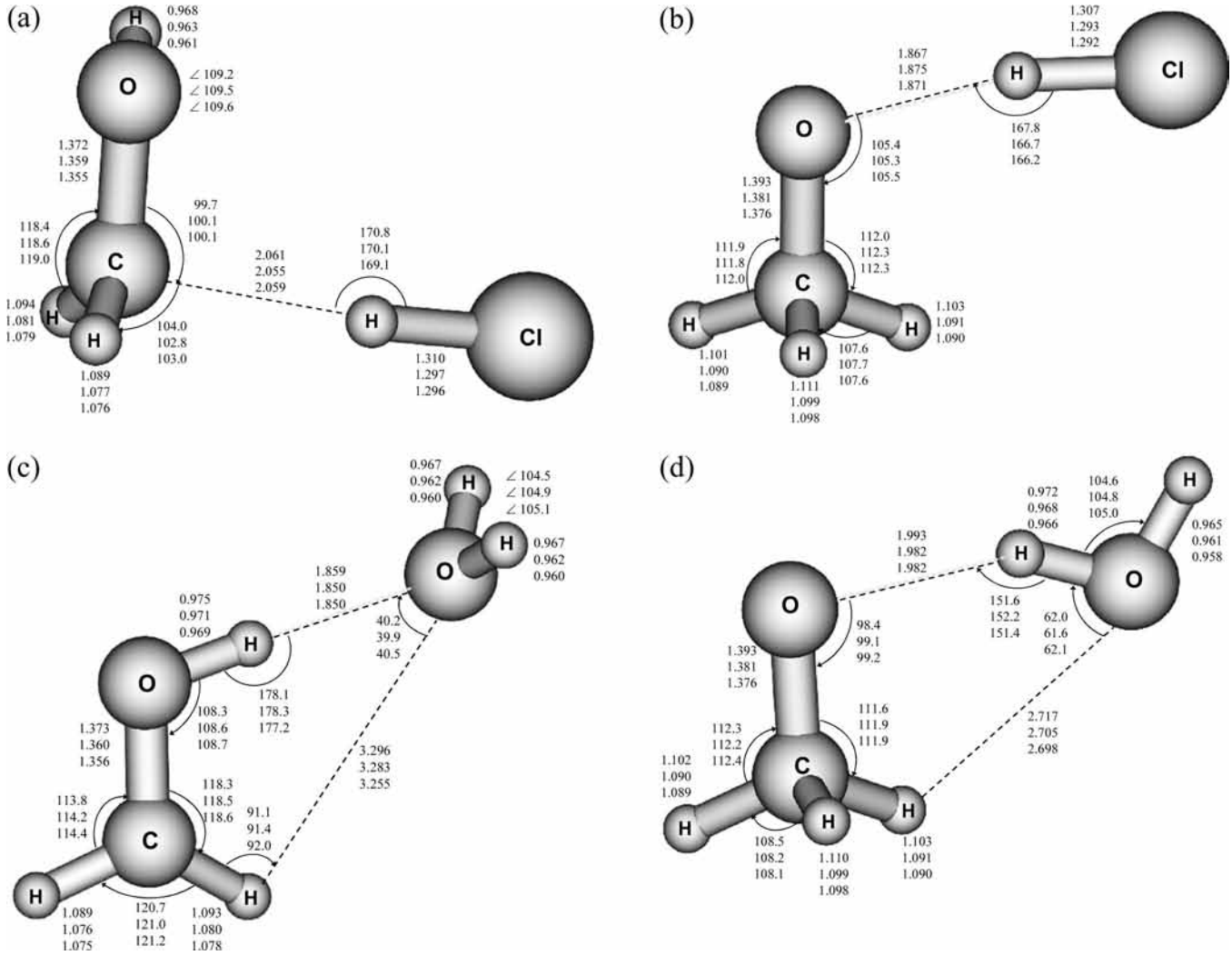

Figure 6. Structures and geometrical parameters of the postreaction complexes of the reactions (a) $CH_3OH + Cl \rightarrow CH_2OH + HCl$, (b) $CH_3OH + Cl \rightarrow CH_3O + HCl$, (c) $CH_3OH + OH \rightarrow CH_2OH + H_2O$, and (d) $CH_3OH + OH \rightarrow CH_3O + H_2O$ calculated at the MP2/aug-cc-pVDZ (top values), MP2/aug-cc-pVTZ, and MP2/aug-cc-pVQZ (bottom values) levels of theory, respectively. Bond lengths are in Angström and bond angles are in degrees.

the experimental values for the OH reaction with CH_3OH is shown in Figure 10. Like for the reaction with Cl, the effect of spin−orbit coupling of the OH radical was taken into account for the calculation of the rate coefficients. The electronic barrier was increased by 0.8 kJ/mol according to the calculated spin−orbit coupling at the stationary points. For the methoxy product channel, the spin−orbit splitting of 134 cm^{-1} in the ground X^2E electronic state of CH_3O[122] has not been taken into account. In its ground electronic state, CH_3O exhibits a Jahn−Teller effect with a stabilization energy of 270 cm^{-1}.[122] The Jahn−Teller distortions which lead to an equilibrium geometry of C_s symmetry corresponding to a Jahn−Teller minimum can quench the electronic angular momentum and thus reduce the spin−orbit splitting.[123] In contrast to the calculations of the Cl reaction with CH_3OH where the harmonic oscillator approximation was applied for all frequencies, in the calculation of the rate coefficients for the OH reactions the internal C···H···OH torsional modes for both product channels were treated as a hindered rotor. As can be seen from Figure 10, our CVT/SCT calculations within the ISPE model give rate coefficients in excellent agreement with experimental data.[113,114] Table 2 shows the calculated rate coefficients, $k = k_{17a} + k_{17b}$ and k_{17b} as well as the branching ratio, $k_{17b}/(k_{17a} + k_{17b})$, for the methoxy channel in comparison to experimental branching

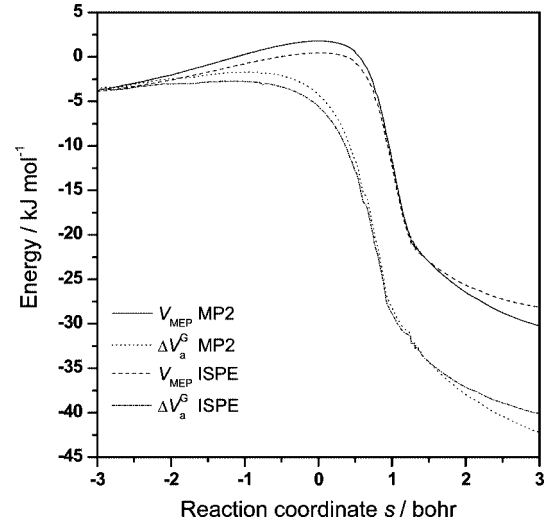

Figure 7. Minimum energy path, V_{MEP}, and vibrationally adiabatic ground-state potential energy curve, ΔV_a^G, as a function of the reaction coordinate, s, for the reaction $CH_3OH + Cl \rightarrow CH_2OH + HCl$ calculated at the MP2/aug-cc-pVTZ level of theory without and with dual-level reaction path dynamics by interpolated single-point energies (ISPE) where the contribution of spin−orbit coupling has been included. All quantities are with respect to the reactants.

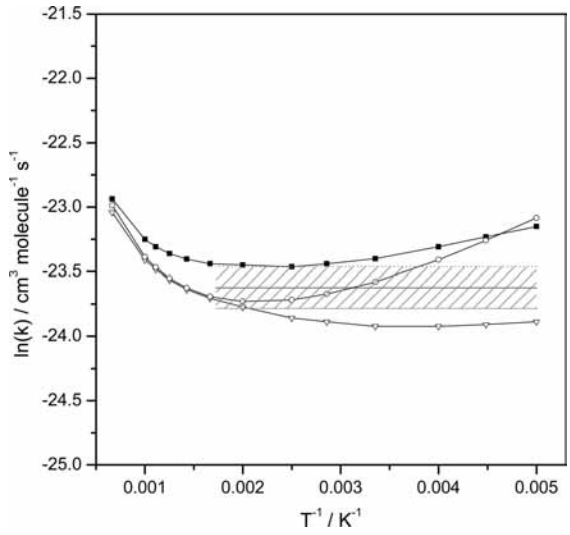

Figure 8. Arrhenius plot of calculated and experimental rate coefficients for the reaction $CH_3OH + Cl \rightarrow CH_2OH + HCl$. (-■-) This work, TST with MP2/aug-cc-pVTZ data. (−○−)This work, ICVT/SCT with ISPE including spin−orbit (SO). coupling. (-▽-) This work, ICVT/SCT with MP2/aug-cc-pVTZ data. (−) Atkinson et al.,[69] evaluation of reference data with uncertainty limits.

ratios. The recommended branching ratio $k_{17b}/k = 0.15 \pm 0.10$ at 298 K[114] for the methoxy channel is mainly based on the measurements of McCaulley et al.[19] Other experimental measurements at 298 K performed by Meier et al.[102] ($k_{17b}/k_{17} = 0.17 \pm 0.13$ and 0.25 ± 0.08) and Hägele et al.[104] are within the recommended range. Hägele et al. also report a branching ratio of $k_{17b}/k = 0.22 \pm 0.07$ at 393 K and suggest that the two abstraction channels become equally important at approximately 780 K, an estimation which is confirmed by Hess and Tully[18] who estimate that nearly half of the reactivity proceeds through the methoxy channel at 860 K. Dóbé et al.[115] found branching ratios of $k_{17b}/k_{17} = 0.15 \pm 0.05$ and 0.29 at 482 and 612 K, respectively. The branching ratios we obtained are in good agreement with the caluclations of Xu and Lin[30] who report values of $k_{17b}/k_{17} = 0.03-0.07$ between 200 and 1500 K and of Jodkowski et al.[31] ($k_{17b}/k_{17} = 0.06$ in the temperature range 300−1000 K). Galano et al.[29] report a significantly larger branching ratio of 0.36 at 298 K.

3.4. Kinetic Isotope Effects. The ^2H, ^{13}C, and ^{18}O kinetic isotope effects in the Cl and OH reaction with CH_3OH at room temperature are given in comparison to experimental data in Table 3. Table 4 shows the CH_3OH/CD_3OH KIEs in the OH reaction with methanol over a temperature range of 294−864 K in comparison to experimental measurements. The corresponding calculated KIEs in the temperature range of 200−1500 K are available in Tables S5−S9 (Supporting Information). As can be seen from Tables 1, 3, and 4, the reactions proceed more slowly for all the heavy isotopologues than for CH_3OH with both Cl and OH radicals. This is the expected kinetic isotope effect (KIE), in which the change in zero point energy upon substitution with a heavy isotope decreases the reaction rate. Substitution with deuterium leads to large KIEs, which is expected as this represents the largest relative change in mass. Also, tunnelling in the H-abstraction is expected to be more important for H than for D, which may in part explain why the reaction of CH_3OH is a factor of 3.011 faster for Cl and 2.566 faster for OH than that of CD_3OH. A further analysis of the tunneling contribution to the KIEs will be given later. Inspecting Tables 3 and 4 shows that our (I)CVT/SCT calculations of the d3 KIEs(CH_3OH/CD_3OH) underestimate the experimental KIEs at room temperature for both reactions. For the OH reaction with methanol, the d3 KIEs in the temperature range $T > 300$ K on the MP2/aug-cc-pVTZ PES are in good agreement with the experimental data reported by Hess and Tully,[18] whereas the KIEs obtained with the ISPE model underestimate the experimental data over the whole temperature range of 294−864 K (see Table 4). It is interesting that the experimental d3 KIE in the Cl reaction is rather well reproduced when applying the TST method within the ISPE model (see Table S5, Supporting Information). The KIE(CH_3OH/CHD_2OH) in the Cl reaction calculated with the ICVT/SCT method is in reasonable agreement with experimental data. In the OH reaction, the d2 KIE is predicted to be too high compared to the experiment, a finding which is also made for the d1 KIE(CH_3OH/CH_2DOH) for both reactions.

The ^{13}C and ^{18}O isotope effects are more subtle compared to the ^2H KIEs, and both KIEs are twice as large for Cl as for OH as can be seen from the experimental results given in Table 1. The origin of this general difference in the KIEs might lie in the simple fact that the potential energy surfaces of the two reactions are quite different—the OH reaction is more exothermic than the Cl reaction by ca. 65 kJ/mol for the dominating hydroxymethyl channel (see Tables S1 and S3, Supporting Information). Complex-forming reactions exhibit an unusual isotope effect as seen for the CO + OH reaction and the reactions of HCHO with various radicals.[35,124] The ^{18}O isotope effects are very small, as this atom is not directly involved in the bond being broken during the reaction for the main channel 17a and 18a. However, the fact that there is a measurable ^{18}O KIE in both the Cl and in the OH reaction may be taken as an indirect confirmation of the formation of a prereaction adduct, as is confirmed by the theoretical calculations of the stationary points on the MEP of all reactions. Comparison with the theoretical determinations of the KIEs in Table 3 shows that the experimental ^{13}C KIE for the OH reaction is well reproduced when applying the ISPE model. As can be seen from Table S8 (Supporting Information), the TST model predicts inverse KIEs almost in the whole temperature range 200−1500 K. In the Cl reaction, the experimental ^{13}C KIE is underestimated with all models. The same can be said for the ^{18}O KIE. However, the ICVT/SCT calculations on the MP2 PES and applying dual level corrections predict, for both the ^{13}C and ^{18}O, KIEs greater than one over the whole temperature range (see Table S8, Supporting Information). In contrast, in the OH reaction, the CVT/SCT as well as the TST calculations for the MP2 and ISPE models predict inverse ^{18}O KIEs almost for the whole temperature range (see Table S9, Supporting Information), in contradiction to experimental measurements. Only the KIEs calculated on the MP2 PES applying the CVT/SCT method are correctly predicted larger than one between 200 and 298 K, resulting in a calculated KIE($CH_3{}^{16}OH/CH_3{}^{18}OH$). that is in good agreement with experiment at room temperature. In general, inspection of Table 3 and Tables S5−S9 (Supporting Information) shows that in the Cl reaction the single-point energy corrections of the PES in the dual level calculations have virtually no effect on the calculated KIEs, whereas in the OH reaction the KIEs calculated with the ISPE model are significantly lower compared to those calculated on the MP2 PES.

To analyze the theoretically determined kinetic isotope effects in more detail, a factor analysis as described in refs 125 and

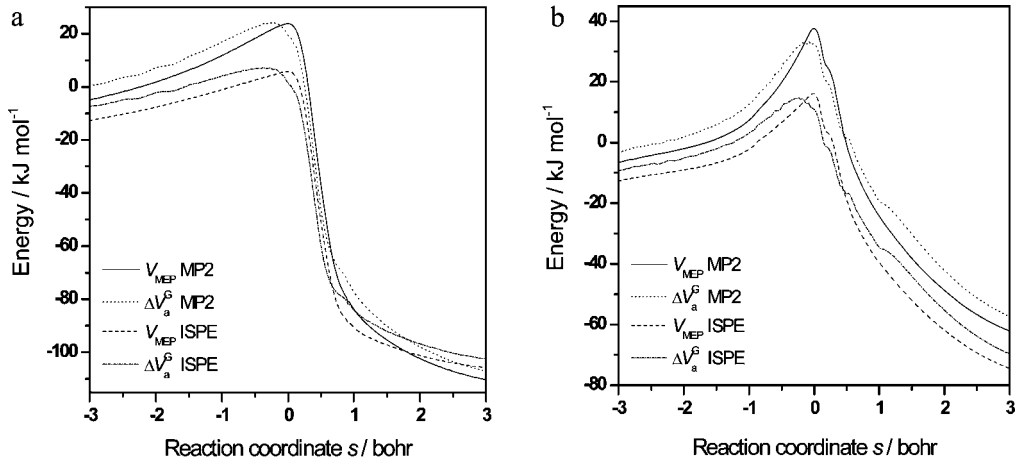

Figure 9. Minimum energy path, V_{MEP}, and vibrationally adiabatic ground-state potential energy curve, ΔV_a^G, as a function of the reaction coordinate, s, for the reaction (a) $CH_3OH + OH \rightarrow CH_2OH + H_2O$ and (b) $CH_3OH + OH \rightarrow CH_3O + H_2O$ calculated at the MP2/aug-cc-pVTZ level of theory without and with dual-level reaction path dynamics by interpolated single-point energies (ISPE) where the contribution of spin−orbit coupling has been included. All quantities are with respect to the reactants.

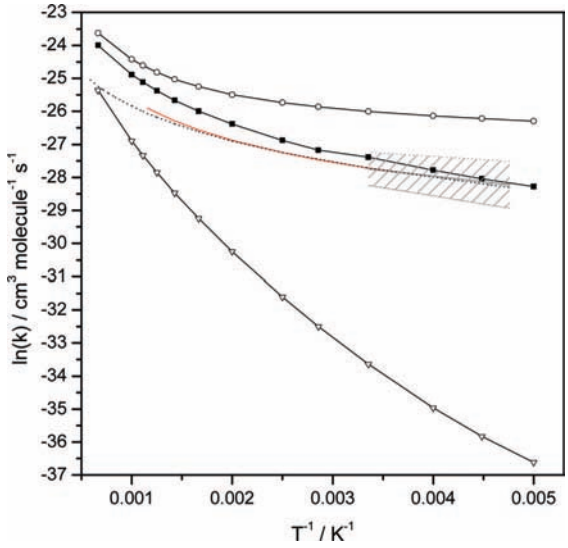

Figure 10. Arrhenius plot of calculated and experimental overall rate coefficients for the reaction of CH_3OH with the OH radical. (-○-) TST with ISPE including spin−orbit (SO) coupling. (-■-) CVT/SCT with ISPE including SO coupling. (-▽-) CVT/SCT with MP2/aug-cc-pVTZ data. (—) Atkinson et al.[114] evaluation of reference data with uncertainty limits. (red —) Atkinson et al.[114] evaluation of reference data with a three-parameter expression. (···) Srinivasan et al.[113] experimental data in the temperature range 210−1710 K.

126 was performed but limited to investigations of the variational effect and the tunneling contribution only

$$\mathrm{KIE} = \frac{k_{\mathrm{light}}}{k_{\mathrm{heavy}}} = \eta_{\mathrm{trans}}\eta_{\mathrm{rot}}\eta_{\mathrm{vib}}\eta_{\mathrm{tun}}\eta_{\mathrm{var}} \propto \eta_{\mathrm{tun}}\eta_{\mathrm{var}} \qquad (23)$$

The tunneling contribution is given as $\eta_{tun} = \kappa^{SCT}(\mathrm{light})/\kappa^{SCT}(\mathrm{heavy})$, i.e., the ratio of the tunneling factors for the light and the heavy isotopologue, and the variational effect is given as $\eta_{var} = \mathrm{KIE}^{(I)CVT}/\mathrm{KIE}^{TST}$, i.e., the ratio of KIEs calculated using variational and conventional transition state theory.

In the case of the $CH_3OH + Cl$ reaction, the factor analysis showed that a moderate variational effect can be found for the CH_3OH/CD_3OH KIE in the present study: $\eta_{var}(200\ \mathrm{K}) = 0.59$ (0.63), $\eta_{var}(298\ \mathrm{K}) = 0.76$ (0.79), $\eta_{var}(500\ \mathrm{K}) = 0.96$ (0.97) for the ISPE and MP2 (values in parentheses) models, respectively (see Table S10, Supporting Information). This variational effect is further lowered for the di- and monodeuterated KIEs

TABLE 2: Rate Coefficients, $k = k_{17a} + k_{17b}$ and k_{17b}, Calculated at the CVT/SCT Level of Theory and Theoretical Branching Ratios of the Methoxy Reaction Channel, k_{17b}/k, for the $CH_3OH + OH$ Reaction in Comparison to Experimental Branching Ratios

T (K)	$k = k_{17a} + k_{17b}$ (cm^3 molecule^{-1} s^{-1})	k_{17b} (cm^3 molecule^{-1} s^{-1})	branching ratio k_{17b}/k calcd	branching ratio k_{17b}/k exptl
200	5.23×10^{-13}	1.85×10^{-14}	0.04	
223	6.63×10^{-13}	2.14×10^{-14}	0.03	
250	8.57×10^{-13}	2.57×10^{-14}	0.03	
298	1.28×10^{-12}	3.63×10^{-14}	0.03	$0.15 \pm 0 \times 10^{114}$ 0.11 ± 0.03^{104} 0.17 ± 0.13^{a} 0.25 ± 0.08^{b}
350	1.57×10^{-12}	4.64×10^{-14}	0.03	
400	2.12×10^{-12}	6.48×10^{-14}	0.03	0.22 ± 0.07^{c}
500	3.48×10^{-12}	1.18×10^{-13}	0.03	0.15 ± 0.05^{d}
600	5.13×10^{-12}	1.48×10^{-13}	0.03	0.29^{e}
700	7.16×10^{-12}	2.29×10^{-13}	0.03	
800	9.55×10^{-12}	3.36×10^{-13}	0.04	
900	1.23×10^{-11}	4.72×10^{-13}	0.04	
1000	1.55×10^{-11}	6.40×10^{-13}	0.04	
1500	3.77×10^{-11}	2.04×10^{-12}	0.05	

[a] Ref 102 with discharge flow laser-excited fluorescence. [b] Ref 102 with discharge mass spectrometry. [c] Ref 104 at 393 K. [d] Ref 115 at 482 K. [e] Ref 115 at 612 K.

with $\eta_{var}(200\ \mathrm{K}) = 0.82$ and $\eta_{var}(500\ \mathrm{K}) = 0.99$ for KIE(CH_3OH/CHD_2OH) and the ISPE model and with $\eta_{var}(200\ \mathrm{K}) = 0.93$ and $\eta_{var}(500\ \mathrm{K}) = 1.00$ for KIE(CH_3OH/CH_2DOH) and the ISPE model (see Tables S11 and S12, Supporting Information). For the carbon-13 and oxygen-18 KIEs, virtually no variational effects can be observed: $\eta_{var}(200\ \mathrm{K}) = 1.005$ and 1.001 and $\eta_{var}(500\ \mathrm{K}) = 1.001$ and 1.005 for KIE($^{12}C/^{13}C$) and KIE($^{16}O/^{18}O$), respectively (see Tables S13 and S14, Supporting Information). No tunneling contributions are found for any of the KIEs (see Tables S10−S14, Supporting Information).

The factor analysis of the KIEs in the OH reaction shows a less distinct pattern for the variational effects and tunneling contributions. In the calculation of the $^{12}C/^{13}C$ ratio within the ISPE model which gives results in good agreement with experiment, the variational effect slightly dominates over the tunneling contribution over the whole temperature range. When applying the MP2 PES, the tunneling contribution dominates up to 500 K ($\eta_{tun} = 1.13$ and 1.02 at 200 and 500 K compared to $\eta_{var} = 1.02$ and 1.01 at 200 and 500 K, respectively). In the higher temperature range, the variational effect becomes slightly

TABLE 3: Kinetic Isotope Effects, $\alpha = k_{light}/k_{heavy}$, in the Reaction of CH_3OH with Cl Atoms and OH Radicals at 298 K[a]

isotopologue	Cl reaction			OH reaction		
	MP2	ISPE	experiment	MP2	ISPE	experiment
	ICVT/SCT			CVT/SCT		
CH_3OH/CD_3OH	2.099	2.063	3.011 ± 0.059[b]	2.307	1.836	2.566 ± 0.042[b] 2.15 ± 0.13[c] 3.35 ± 0.72[d] 1.65[e]
CH_3OH/CHD_2OH	1.589	1.572	1.536 ± 0.060[b]	1.580	1.423	1.326 ± 0.021[b]
CH_3OH/CH_2DOH	1.236	1.236	1.162 ± 0.022[b]	1.214	1.171	1.119 ± 0.045[b]
$^{12}CH_3OH/^{13}CH_3OH$	1.007	1.009	1.055 ± 0.016[b]	1.058	1.038	1.031 ± 0.020[b]
$CH_3{}^{16}OH/CH_3{}^{18}OH$	1.000	1.000	1.025 ± 0.022[b]	1.009	0.991	1.017 ± 0.012[b]

[a] The reaction rates are obtained by direct variational transition state theory with interpolated single-point energies (ISPE) dynamics calculations based on electronic structure information at the MP2/aug-cc-pVTZ level of theory as explained in the text. KIEs calculated with improved canonical variational transition state theory (ICVT) and canonical variational transition state theory (CVT) with small-curvature tunneling (SCT) are compared with experimental measurements. [b] This work. [c] Ref 18. [d] Ref 19 at 294 K. [e] Ref 20 at 293 K.

TABLE 4: CH_3OH/CD_3OH Kinetic Isotope Effects, $\alpha = k_{light}/k_{heavy}$, in the Reaction of Methanol with Hydroxyl Radicals in Comparison to Experimental Measurements[a]

T (K)	MP2 CVT/SCT	ISPE CVT/SCT	experiment[b]
294	2.339	1.835	2.15 ± 0.13, 3.35 ± 0.72[c], 1.65[d]
298	2.307	1.836	2.566 ± 0.042[e]
331	2.078	1.761	2.06 ± 0.12
382	1.863	1.433	1.95 ± 0.12
440	2.020	1.372	1.84 ± 0.11
529	1.823	1.306	1.81 ± 0.12
634	1.681	1.471	1.72 ± 0.10
730	1.573	1.432	1.52 ± 0.10
864	1.468	1.368	1.27 ± 0.09

[a] The reaction rates are obtained by direct variational transition state theory with interpolated single-point energies (ISPE) dynamics calculations based on electronic structure information at the MP2/aug-cc-pVTZ level of theory as explained in the text. KIEs calculated with canonical variational transition state theory with small-curvature tunneling (CVT/SCT) are compared with experimental measurements. [b] Ref 18. [c] Ref 19. [d] Ref 20 at 293 K. [e] This work.

dominant (see Table S18, Supporting Information). A similar picture can be found for the $^{16}O/^{18}O$ KIEs: in the ISPE model, variational effect and tunneling contribution are of almost the same magnitude, whereas for the calculations on the MP2 PES the tunneling contribution is slightly dominating over the variational effect (see Table S19, Supporting Information). For the d3 KIE(CH_3OH/CD_3OH), a large dominant variational effect of $\eta_{var}(200\ K) = 0.19\ (0.23)$, $\eta_{var}(298\ K) = 0.35\ (0.37)$, and $\eta_{var}(800\ K) = 0.72\ (0.76)$ can be found for the ISPE and MP2 (in parentheses) models, respectively (see Table S15, Supporting Information). This effect decreases considerably for the di- and monodeuterated KIEs with values of $\eta_{var}(200\ K) = 0.71$ and 0.94 and $\eta_{var}(800\ K) = 0.85$ and 0.94 for KIE(CH_3OH/CHD_2OH) and KIE(CH_3OH/CH_2DOH), respectively, when applying the ISPE model (see Tables S16 and S17, Supporting Information). The factor analysis shows appreciable tunneling effects only for the KIE(CH_3OH/CD_3OH) for calculations on the MP2 PES. For the ISPE model an unexpected tunneling contribution with $\eta_{tun} < 1$ is observed, a finding which is also found for the tunneling contribution of the di- and monodeuterated KIEs, for both the MP2 and ISPE calculations (see Tables S15−S17, Supporting Information). Table S20 (Supporting Information) shows the tunneling contributions, $k^{CVT}/k^{CVT/SCT}$, in the calculation of the rate coefficients of the OH reaction with CH_3OH and CD_3OH. It can be seen that the calculations based on the MP2/aug-cc-pVTZ PES predict larger tunneling contributions for the perprotic reaction, whereas in the ISPE model tunneling is larger for the perdeuterated species. Normally one expects tunneling to be more important for the lighter hydrogen than for deuterium as was found in our experimental study. From Figure 9, it can be seen that the vibrationally adiabatic ground-state potential energy curve, ΔV_a^G, is drastically reduced when applying the single-point energy corrections in the ISPE dual level model. In such a low-barrier reaction, isotopic substitution changes ΔV_a^G in a relatively drastic way, resulting in larger tunneling probabilities for the C−D abstraction reaction compared to the C−H abstraction reaction. This effect is less pronounced for ΔV_a^G on the MP2 surface which has a considerably larger barrier height. Obviously, the small curvature tunneling approximation used in the present study is not able to describe tunneling properly for all systems: the "corner cutting effect" for the reactions takes place over a larger part of the reaction swath than the SCT approximation is able to describe.[57,59,127]

4. Conclusions

We present measurements of the isotopic signatures of the reactions of CH_3OH, CH_2DOH, CHD_2OH, CD_3OH, $^{13}CH_3OH$, and $CH_3{}^{18}OH$ with Cl and hydroxyl radicals. The deuterium isotope effects are the largest due to the impact of D substitution on the ZPE/activation barrier and on the tunneling rates. The chlorine reactions exhibit somewhat larger KIEs than the OH reactions. The KIEs of CH_3OH can be compared to those for methane, which have been the subject of several studies,[124,128,129] and chloromethane,[130] whose KIEs in the reactions with Cl and OH are included in Table 1 for comparison. As can be seen, the trends are similar. However, the KIEs for CD_4 in both the Cl and OH reactions are significantly larger than for CD_3OH. The fact that substituted methanes facilitate the abstraction of deuterium compared to CD_4 has recently been observed in methyl chloride.[130] Hydrogen abstraction from the OH group in methanol might explain why the KIE is smallest in methanol. As seen in Table 1, the $^{12}C/^{13}C$ KIE in the OH reaction of CH_3OH and CH_3Cl are an order of magnitude larger than for CH_4. Sellevåg et al.[131] suggested in their study of the ^{13}C and deuterium KIEs in the Cl and OH reactions of CH_4 and CH_3Cl that the order of magnitude difference in the $^{12}C/^{13}C$ KIEs of the OH reaction with methane and chloromethane is due to the difference in barrier height of the C···H···OH torsional mode which contributes to the $^{12}C/^{13}C$ kinetic isotope effect. They assumed that this description also applies to the $CH_3OH + OH$ reaction. We calculated a barrier height of the torsional mode of 499 cm^{-1} for the transition state of the dominating C−H abstraction reaction which is comparable to the 303 cm^{-1}

calculated by Sellevåg et al.[131] for the corresponding torsional mode in the $CH_3Cl\cdots OH$ transition state and which was also treated as a hindered rotor.

On the basis of the results of this work, the deuteric kinetic isotope effects in the Cl and OH reaction of methanol can largely be explained by mainly variational effects. Tunneling contributions are only of minor importance in the OH reaction: for the almost barrierless Cl reaction, no tunneling contributions in the kinetic isotope effects are found.

The theoretical study of the kinetics of hydrogen abstraction from methanol by chlorine and the hydroxyl radical predict for all reaction channels pre- and postreaction adducts on the potential energy curves. For both the chlorine and hydroxyl radical reactions, the product channel leading to the hydroxymethyl radical is the dominant reaction path with significantly lower barrier heights compared to the methoxy radical product channel.

These isotopic signatures verified experimentally and theoretically can be used for tracing the atmospheric pathways, sources, and sinks of methanol, a method which has been successfully employed for other atmospheric trace species.

Acknowledgment. This work is part of the ACTION (Atmospheric Chemistry and Transport from Isotopic Analysis) project supported by the Norwegian Research Council. The experiments were made possible by a researcher mobility grant from the Nordic Network for Chemical Kinetics supported by the Nordic Academy for Advanced study (NorFA) and by the financial support of the Danish Natural Science Research Council. The authors would like to thank Flemming M. Nicolaisen for his valuable assistance in recording the high-resolution spectra of the methanol isotopologue.

Supporting Information Available: Facsimile model of the $OH + CH_3OH$ reaction system (Figure S1). Structures and geometrical parameters of the CH_2OH radical, the CH_3O radical, and CH_3OH (Figure S2). Generalized normal-mode vibrational frequencies as a function of the reaction coordinate, *s*, for the reaction $CH_3OH + Cl \rightarrow CH_2OH + HCl$ (Figure S3). Arrhenius plot of calculated rate coefficients for the reaction $CH_3OH + Cl \rightarrow CH_3O + HCl$ (Figure S4). Born−Oppenheimer and zero-point corrected energies of stationary points involved in the reactions $CH_3OH + Cl \rightarrow CH_2OH + HCl$ (Table S1), $CH_3OH + Cl \rightarrow CH_3O + HCl$ (Table S2), $CH_3OH + OH \rightarrow CH_2OH + H_2O$ (Table S3), and $CH_3OH + OH \rightarrow CH_3O + H_2O$ (Table S4). CH_3OH/CD_3OH kinetic isotope effects in the reaction of CH_3OH with Cl atoms and OH radicals (Table S5). CH_3OH/CHD_2OH kinetic isotope effects in the reaction of CH_3OH with Cl atoms and OH radicals (Table S6). CH_3OH/CH_2DOH kinetic isotope effects in the reaction of CH_3OH with Cl atoms and OH radicals (Table S7). $^{12}CH_3OH/^{13}CH_3OH$ kinetic isotope effects in the reaction of CH_3OH with Cl atoms and OH radicals (Table S8). $CH_3{}^{16}OH/CH_3{}^{18}OH$ kinetic isotope effects in the reaction of CH_3OH with Cl atoms and OH radicals (Table S9). Factor analysis of the kinetic isotope effects CH_3OH/CD_3OH in the reaction of methanol with chlorine (Table S10). Factor analysis of the kinetic isotope effects CH_3OH/CHD_2OH in the reaction of methanol with chlorine (Table S11). Factor analysis of the kinetic isotope effects CH_3OH/CH_2DOH in the reaction of methanol with chlorine (Table S12). Factor analysis of the kinetic isotope effects $^{12}CH_3OH/^{13}CH_3OH$ in the reaction of methanol with chlorine (Table S13). Factor analysis of the kinetic isotope effects $CH_3{}^{16}OH/CH_3{}^{18}OH$ in the reaction of methanol with chlorine (Table S14). Factor analysis of the kinetic isotope effects CH_3OH/CD_3OH in the reaction of methanol with hydroxyl radicals (Table S15). Factor analysis of the kinetic isotope effects CH_3OH/CHD_2OH in the reaction of methanol with hydroxyl radicals (Table S16). Factor analysis of the kinetic isotope effects CH_3OH/CH_2DOH in the reaction of methanol with hydroxyl radicals (Table S17). Factor analysis of the kinetic isotope effects $^{12}CH_3OH/^{13}CH_3OH$ in the reaction of methanol with hydroxyl radicals (Table S18). Factor analysis of the kinetic isotope effects $CH_3{}^{16}OH/CH_3{}^{18}OH$ in the reaction of methanol with hydroxyl radicals (Table S19). Tunneling contributions in the calculation of the rate coefficients of the OH reaction with CH_3OH and CD_3OH (Table S20). This material is available free of charge via the Internet at http://pubs.acs.org.

References and Notes

(1) Heikes, B. G.; Chang, W. N.; Pilson, M. E. Q.; Swift, E.; Singh, H. B.; Guenther, A.; Jacob, D. J.; Field, B. D.; Fall, R.; Riemer, D.; Brand, L. *Global Biogeochem. Cycles* **2002**, *16*, 1133.

(2) Harley, P.; Greenberg, J.; Niinemets, U.; Guenther, A. *Biogeosciences* **2007**, *4*, 1083.

(3) Singh, H.; Chen, Y.; Staudt, A.; Jacob, D.; Blake, D.; Heikes, B.; Snow, J. *Nature (London, United Kingdom)* **2001**, *410*, 1078.

(4) Singh, H.; Chen, Y.; Tabazadeh, A.; Fukui, Y.; Bey, I.; Yantosca, R.; Jacob, D.; Arnold, F.; Wohlfrom, K.; Atlas, E.; Flocke, F.; Blake, D.; Blake, N.; Heikes, B.; Snow, J.; Talbot, R.; Gregory, G.; Sachse, G.; Vay, S.; Kondo, Y. *J. Geophys. Res. [Atmospheres]* **2000**, *105*, 3795.

(5) Singh, H. B.; Salas, L. J.; Chatfield, R. B.; Czech, E.; Fried, A.; Walega, J.; Evans, M. J.; Field, B. D.; Jacob, D. J.; Blake, D.; Heikes, B.; Talbot, R.; Sachse, G.; Crawford, J. H.; Avery, M. A.; Sandholm, S.; Fuelberg, H *J. Geophys. Res. [Atmospheres]* **2004**, *109*, D15S07.

(6) Monod, A.; Chebbi, A.; Durand-Jolibois, R.; Carlier, P. *Atmos. Environ.* **2000**, *34*, 5283.

(7) Allan, W.; Lowe, D. C.; Cainey, J. M. *Geophys. Res. Lett.* **2001**, *28*, 3239.

(8) Tyndall, G. S.; Wallington, T. J.; Ball, J. C. *J. Phys. Chem. A* **1998**, *102*, 2547.

(9) Brenninkmeijer, C. A. M.; Janssen, C.; Kaiser, J.; Roeckmann, T.; Rhee, T. S.; Assonov, S. S *Chem. Rev.* **2003**, *103*, 5125.

(10) Quay, P.; Stutsman, J.; Wilbur, D.; Snover, A.; Dlugokencky, E.; Brown, T. *Global Biogeochem. Cycles* **1999**, *13*, 445.

(11) McCarthy, M. C.; Boering, K. A.; Rice, A. L.; Tyler, S. C.; Connell, P.; Atlas, E. *J. Geophys. Res. [Atmospheres]* **2003**, *108*, ACH12/1.

(12) Röckmann, T.; Brenninkmeijer, C. A. M.; Sauerssig, G.; Bergamaschi, P.; Crowley, J. N.; Fischer, H.; Crutzen, P. J. *Science* **1998**, *281*, 544.

(13) Leung, F.-Y. T.; Colussi, A. J.; Hoffmann, M. R.; Toon, G. C *Geophys. Res. Lett.* **2002**, *29*, 112–1.

(14) Blake, G. A.; Liang, M.-C.; Morgan, C. G.; Yung, Y. L *Geophys. Res. Lett.* **2003**, *30*, 58–1.

(15) Bhattacharya, S. K.; Savarino, J.; Thiemens, M. H. *Geophys. Res. Lett.* **2000**, *27*, 1459.

(16) Rahn, T.; Eiler, J. M.; Boering, K. A.; Wennberg, P. O.; McCarthy, M. C.; Tyler, S.; Schauffler, S.; Donnelly, S.; Atlas, E. *Nature* **2003**, *424*, 918.

(17) Feilberg, K. L.; Johnson, M. S.; Bacak, A.; Röckmann, T.; Nielsen, C. J. *J. Phys. Chem. A* **2007**, *111*, 9034.

(18) Hess, W. P.; Tully, F. P. *J. Phys. Chem.* **1989**, *93*, 1944.

(19) McCaulley, J. A.; Kelly, N.; Golde, M. F.; Kaufman, F. *J. Phys. Chem.* **1989**, *93*, 1014.

(20) Greenhill, P. G.; O′Grady, B. V. *Aust. J. Chem.* **1986**, *39*, 1775.

(21) Garzon, A.; Cuevas, C. A.; Ceacero, A. A.; Notario, A.; Albaladejo, J.; Fernandez-Gomez, M. *J. Chem. Phys.* **2006**, *125*, 104305–1.

(22) Jodkowski, J. T.; Rayez, M.-T.; Rayez, J.-C.; Berces, T.; Dobe, S. *J. Phys. Chem. A* **1998**, *102*, 9230.

(23) Chen, B. Z.; Huang, M. B. *Chin. Chem. Lett.* **2001**, *12*, 727.

(24) Rudic, S.; Murray, C.; Harvey, J. N.; Orr-Ewing, A. J. *J. Chem. Phys.* **2004**, *120*, 186.

(25) Rudic, S.; Murray, C.; Ascenzi, D.; Anderson, H.; Harvey, J. N.; Orr-Ewing, A. J. *J. Chem. Phys.* **2002**, *117*, 5692.

(26) Kollias, A. C.; Couronne, O.; Lester, W. A., Jr. *J. Chem. Phys.* **2004**, *121*, 1357.

(27) Murray, C.; Orr-Ewing, A. J.; Toomes, R. L.; Kitsopoulos, T. N. *J. Chem. Phys.* **2004**, *120*, 2230.

(28) Ishimoto, T.; Tachikawa, M.; Tokiwa, H.; Nagashima, U. *Chem. Phys.* **2005**, *314*, 231.

(29) Galano, A.; Alvarez-Idaboy, J. R.; Bravo-Perez, G.; Ruiz-Santoyo, M. E. *Phys. Chem. Chem. Phys.* **2002**, *4*, 4648.

(30) Xu, S.; Lin, M. C. *Proc. Comb. Instit.* **2007**, *31*, 159.

(31) Jodkowski, J. T.; Rayez, M.-T.; Rayez, J.-C.; Berces, T.; Dobe, S. *J. Phys. Chem. A* **1999**, *103*, 3750.
(32) Pardo, L.; Banfelder, J. R.; Osman, R. *J. Am. Chem. Soc.* **1992**, *114*, 2382.
(33) Hatipoglu, A.; Cinar, Z. *THEOCHEM* **2003**, *631*, 189.
(34) Jasper, A. W.; Klippenstein, S. J.; Harding, L. B.; Ruscic, B. *J. Phys. Chem. A* **2007**, *111*, 3932.
(35) Feilberg, K. L.; Johnson, M. S.; Nielsen, C. J. *J. Phys. Chem. A* **2004**, *108*, 7393.
(36) Esler, M. B.; Griffith, D. W. T.; Wilson, S. R.; Steele, L. P. *Anal. Chem.* **2000**, *72*, 216.
(37) Esler, M. B.; Griffith, D. W. T.; Wilson, S. R.; Steele, L. P. *Anal. Chem.* **2000**, *72*, 206.
(38) Griffith, D. W. T. *Appl. Spectrosc.* **1996**, *50*, 59.
(39) Rothman, L. S.; Jacquemart, D.; Barbe, A.; Benner, D. C.; Birk, M.; Brown, L. R.; Carleer, M. R.; Chackerian, C.; Chance, K.; Coudert, L. H.; Dana, V.; Devi, V. M.; Flaud, J. M.; Gamache, R. R.; Goldman, A.; Hartmann, J. M.; Jucks, K. W.; Maki, A. G.; Mandin, J. Y.; Massie, S. T.; Orphal, J.; Perrin, A.; Rinsland, C. P.; Smith, M. A. H.; Tennyson, J.; Tolchenov, R. N.; Toth, R. A.; Vander Auwera, J.; Varanasi, P.; Wagner, G. *J. Quant. Spectrosc. Radiat. Transfer* **2005**, *96*, 139.
(40) Aker, P. M.; Sloan, J. J. *J. Chem. Phys.* **1986**, *85*, 1412.
(41) Huang, Y.; Gu, Y.; Liu, C.; Yang, X.; Tao, Y. *Chem. Phys. Lett.* **1986**, *127*, 432.
(42) Streit, G. E.; Whitten, G. Z.; Johnston, H. S. *Geophys. Res. Lett.* **1976**, *3*, 521.
(43) D′Ottone, L.; Bauer, D.; Campuzano-Jost, P.; Fardy, M.; Hynes, A. J. *Phys. Chem. Chem. Phys.* **2004**, *6*, 4276.
(44) Møller, C.; Plesset, M. S. *Phys. Rev.* **1934**, *46*, 618.
(45) Raghavachari, K.; Trucks, G. W.; Pople, J. A.; Head-Gordon, M. *Chem. Phys. Lett.* **1989**, *157*, 479.
(46) Frisch, M. J.; Trucks, G. W.; Schlegel, H. B.; Scuseria, G. E.; Robb, M. A.; Cheeseman, J. R. ; Montgomery J.A., Jr.; Vreven, T.; Kudin, K. N.; Burant, J. C.; Millam, J. M.; Iyengar, S. S.; Tomasi, J.; Barone, V.; Mennucci, B.; Cossi, M.; Scalmani, G.; Rega, N.; Petersson, G. A.; Nakatsuji, H.; Hada, M.; Ehara, M.; Toyota, K.; Fukuda, R.; Hasegawa, J.; Ishida, M.; Nakajima, T.; Honda, Y.; Kitao, O.; Nakai, H.; Klene, M.; Li, X.; Knox, J. E.; Hratchian, H. P.; Cross, J. B.; Bakken, V.; Adamo, C.; Jaramillo, J.; Gomperts, R.; Stratmann, R. E.; Yazyev, O.; Austin, A. J.; Cammi, R.; Pomelli, C.; Ochterski, J. W.; Ayala, P. Y.; Morokuma, K.; Voth, G. A.; Salvador, P.; Dannenberg, J. J.; Zakrzewski, V. G.; Dapprich, S.; Daniels, A. D.; Strain, M. C.; Farkas, O.; Malick, D. K.; Rabuck, A. D.; Raghavachari, K.; Foresman, J. B.; Ortiz, J. V.; Cui, Q.; Baboul, A. G.; Clifford, S.; Cioslowski, J.; Stefanov, B. B.; Liu, G.; Liashenko, A.; Piskorz, P.; Komaromi, I.; Martin, R. L.; Fox, D. J.; Keith, T.; Al.Laham, M. A.; Peng, C. Y.; Nanayakkara, A.; Challacombe, M.; Gill, P. M. W.; Johnson, B.; Chen, W.; Wong, M. W.; Gonzalez, C.; Pople, J. A. *Gaussian, Inc.*; Wallingford, CT, 2004.
(47) Dunning, T. H., Jr. *J. Chem. Phys.* **1989**, *90*, 1007.
(48) Kendall, R. A.; Dunning, T. H., Jr.; Harrison, R. J. *J. Chem. Phys.* **1992**, *96*, 6796.
(49) Halkier, A.; Helgaker, T.; Jorgensen, P.; Klopper, W.; Koch, H.; Olsen, J.; Wilson, A. K. *Chem. Phys. Lett.* **1998**, *286*, 243.
(50) Gonzalez, C.; Schlegel, H. B. *J. Chem. Phys.* **1989**, *90*, 2154.
(51) Gonzalez, C.; Schlegel, H. B. *J. Phys. Chem.* **1990**, *94*, 5523.
(52) Corchado, J. C.; Coitino, E. L.; Chuang, Y.-Y.; Fast, P. L.; Truhlar, D. G. *J. Phys. Chem. A* **1998**, *102*, 2424.
(53) Gonzalez-Lafont, A.; Villa, J.; Lluch, J. M.; Bertran, J.; Steckler, R.; Truhlar, D. G. *J. Phys. Chem. A* **1998**, *102*, 3420.
(54) Chuang, Y.-Y.; Corchado, J. C.; Truhlar, D. G. *J. Phys. Chem. A* **1999**, *103*, 1140.
(55) Corchado, J. C.; Chuang, Y.-Y.; Fast, P. L.; Villà, J.; Hu, W.-P.; Liu, Y.-P.; Lynch, G. C.; Nguyen, K. A.; Jackels, C. F.; Melissas, V. S.; Lynch, B. J.; Rossi, I.; Coitiño, E. L.; Fernandez-Ramos, A.; Ellingson, B. A.; Pu, J.; Albu, T. V.; Zheng, J.; Steckler, R.; Garrett, B. C.; Isaacson, A. D.; Truhlar, D. G. *POLYRATE,* version 9.6; University of Minnesota: Minneapolis, 2007.
(56) Isaacson, A. D.; Sund, M. T.; Rai, S. N.; Truhlar, D. G. *J. Chem. Phys.* **1985**, *82*, 1338.
(57) Truhlar, D. G.; Isaacson, A. D.; Garrett, B. C. Generalized transition state theory. In *The Theory of Chemical Reaction Dynamics*; Baer, M., Ed.; CRC Press: Boca Raton, FL, 1985; Vol. 4; pp 65.
(58) Garrett, B. C.; Truhlar, D. G. *J. Phys. Chem.* **1979**, *83*, 1052.
(59) Liu, Y.-P.; Lynch, G. C.; Truong, T. N.; Lu, D.-H.; Truhlar, D. C.; Garrett, B. C. *J. Am. Chem. Soc.* **1993**, *115*, 2408.
(60) Garrett, B. C.; Truhlar, D. G.; Grev, R. S.; Magnuson, A. W. *J. Phys. Chem.* **1980**, *84*, 1730.
(61) Fast, P. L.; Corchado, J. C.; Truhlar, D. G. *J. Chem. Phys.* **1998**, *109*, 6237.
(62) Villa, J.; Corchado, J. C.; Gonzalez-Lafont, A.; Lluch, J. M.; Truhlar, D. G. *J. Phys. Chem. A* **1999**, *103*, 5061.
(63) Berning, A.; Schweizer, M.; Werner, H. J.; Knowles, P. J.; Palmieri, P. *Mol. Phys.* **2000**, *98*, 1823.
(64) Amos, R. D.; Bernhardsson, A.; Berning, A.; Celani, P.; Cooper, D. L.; Deegan, M. J. O.; Dobbyn, A. J.; Eckert, F.; Hampel, C.; Hetzer, G.; Knowles, P. J.; Korona, T.; Lindh, R.; Lloyd, A. W.; McNicholas, S. J.; Manby, F. R.; Meyer, W.; Mura, M. E.; Nicklass, A.; Palmieri, P.; Pitzer, R.; Rauhut, G.; Schütz, M.; Schumann, U.; Stoll, H.; Stone, A. J.; Tarroni, R.; Thorsteinsson, T.; Werner, H.-J. MOLPRO, a package of ab initio programs designed by H.-J. Werner and P. J. Knowles, version 2002.6, 2002.
(65) Chuang, Y.-Y.; Truhlar, D. G. *J. Chem. Phys.* **2000**, *112*, 1221.
(66) Chuang, Y.-Y.; Truhlar, D. G *J. Chem. Phys.* **2006**, *124*, 179903–1.
(67) Chuang, Y.-Y.; Truhlar, D. G. *J. Chem. Phys.* **2004**, *121*, 7036.
(68) Herron, J. T. *J. Phys. Chem. Ref. Data* **1988**, *17*, 967.
(69) Atkinson, R.; Baulch, D. L.; Cox, R. A.; Crowley, J. N.; Hampson, R. F.; Hynes, R. G.; Jenkin, M. E.; Rossi, M. J.; Troe, J. *Atmos. Chem. Phys.* **2006**, *6*, 3625.
(70) *FACSIMILE for Windows*, Version 4.1.36; MCPA Software Ltd.
(71) NIST Chemical Kinetics Database on the Web, Standard Reference Database 17, version 7.0 (Web Version), release 1.4.1; National Institute of Standards and Technology.
(72) Sander, S. P.; Friedl, R. R.; Golden, D. M.; Kurylo, M. J.; Moortgat, G. K.; Wine, P. H.; Ravishankara, A. R.; Kolb, C. E.; Molina, M. J.; Finlayson-Pitts, B. J.; Huie, R. E.; Orkin, V. L. *Chemical Kinetics and Photochemical Data for Use in Atmospheric Studies. Evaluation Number 15*; National Aeronautics and Space Administration, Jet Propulsion Laboratory, California Institute of Technology: Pasadena, CA, 2006.
(73) Finlayson-Pitts, B. J.; Hernandez, S. K.; Berko, H. N. *J. Phys. Chem.* **1993**, *97*, 1172.
(74) Venkateswarlu, P.; Gordy, W. *J. Chem. Phys.* **1955**, *23*, 1200.
(75) Helgaker, T.; Gauss, J.; Joergensen, P.; Olsen, J. *J. Chem. Phys.* **1997**, *106*, 6430.
(76) Johnson, R. D., III; Hudgens, J. W. *J. Phys. Chem.* **1996**, *100*, 19874.
(77) Bruna, P. J.; Grein, F. *J. Phys. Chem. A* **1998**, *102*, 3141.
(78) Saebo, S.; Radom, L.; Schaefer, H. F., III *J. Chem. Phys.* **1983**, *78*, 845.
(79) Marenich, A. V.; Boggs, J. E. *J. Chem. Phys.* **2003**, *119*, 10105.
(80) Marenich, A. V.; Boggs, J. E *J. Mol. Struct.* **2006**, *780*−*781*, 163.
(81) Galano, A.; Alvarez-Idaboy, J. R. *J. Comput. Chem.* **2006**, *27*, 1203.
(82) Kwok, E. S. C.; Atkinson, R. *Atmos. Environ.* **1995**, *29*, 1685.
(83) Nelson, L.; Rattigan, O.; Neavyn, R.; Sidebottom, H.; Treacy, J. *Int. J. Chem. Kinet.* **1990**, *22*, 1111.
(84) Wu, H.; Mu, Y.; Zhang, X.; Song, W.; Zhou, L. *Huanjing Kexue Xuebao* **2001**, *21*, 649.
(85) Tyndall, G. S.; Orlando, J. J.; Kegley-Owen, C. S.; Wallington, T. J.; Hurley, M. D. *Int. J. Chem. Kinet.* **1999**, *31*, 776.
(86) Ohta, T.; Bandow, H.; Akimoto, H. *Int. J. Chem. Kinet.* **1982**, *14*, 173.
(87) Payne, W. A.; Brunning, J.; Mitchell, M. B.; Stief, L. J. *Int. J. Chem. Kinet.* **1988**, *20*, 63.
(88) Wallington, T. J.; Skewes, L. M.; Siegl, W. O.; Wu, C. H.; Japar, S. M. *Int. J. Chem. Kinet.* **1988**, *20*, 867.
(89) Dobe, S.; Otting, M.; Temps, F.; Wagner, H. G.; Ziemer, H. *Ber. Bunsen-Ges.* **1993**, *97*, 877.
(90) Rudic, S.; Ascenzi, D.; Orr-Ewing, A. J. *Chem. Phys. Lett.* **2000**, *332*, 487.
(91) Ahmed, M.; Peterka, D. S.; Suits, A. G. *Chem. Phys. Lett.* **2000**, *317*, 264.
(92) Smith, J. D.; DeSain, J. D.; Taatjes, C. A. *Chem. Phys. Lett.* **2002**, *366*, 417.
(93) Michael, J. V.; Nava, D. F.; Payne, W. A.; Stief, L. J. *J. Chem. Phys.* **1979**, *70*, 3652.
(94) Lightfoot, P. D.; Veyret, B.; Lesclaux, R. *J. Phys. Chem.* **1990**, *94*, 708.
(95) Ahmed, M.; Peterka, D. S.; Suits, A. G. *Phys. Chem. Chem. Phys.* **2000**, *2*, 861.
(96) Taketani, F.; Takahashi, K.; Matsumi, Y.; Wallington, T. J. *J. Phys. Chem. A* **2005**, *109*, 3935.
(97) Seakins, P. W.; Orlando, J. J.; Tyndall, G. S. *Phys. Chem. Chem. Phys.* **2004**, *6*, 2224.
(98) Bott, J. F.; Cohen, N. *Int. J. Chem. Kinet.* **1991**, *23*, 1075.
(99) Wallington, T. J.; Kurylo, M. J. *Int. J. Chem. Kinet.* **1987**, *19*, 1015.
(100) Osif, T. L.; Simonaitis, R.; Heicklen, J. *J. Photochem.* **1975**, *4*, 233.
(101) Campbell, I. M.; McLaughlin, D. F.; Handy, B. J. *Chem. Phys. Lett.* **1976**, *38*, 362.
(102) Meier, U.; Grotheer, H. H.; Just, T. *Chem. Phys. Lett.* **1984**, *106*, 97.
(103) Meier, U.; Grotheer, H. H.; Riekert, G.; Just, T. *Ber. Bunsen-Ges.* **1985**, *89*, 325.
(104) Haegele, J.; Lorenz, K.; Rhaesa, D.; Zellner, R. *Ber. Bunsen-Ges.* **1983**, *87*, 1023.

(105) Jimenez, E.; Gilles, M. K.; Ravishankara, A. R. *J. Photochem. Photobiol., A: Chem.* **2003**, *157*, 237.
(106) Overend, R.; Paraskevopoulos, G. *J. Phys. Chem.* **1978**, *82*, 1329.
(107) Picquet, B.; Heroux, S.; Chebbi, A.; Doussin, J.-F.; Durand-Jolibois, R.; Monod, A.; Loirat, H.; Carlier, P. *Int. J. Chem. Kinet.* **1998**, *30*, 839.
(108) Dillon, T. J.; Hoelscher, D.; Sivakumaran, V.; Horowitz, A.; Crowley, J. N. *Phys. Chem. Chem. Phys.* **2005**, *7*, 349.
(109) Ravishankara, A. R.; Davis, D. D. *J. Phys. Chem.* **1978**, *82*, 2852.
(110) Tuazon, E. C.; Carter, W. P. L.; Atkinson, R.; Pitts, J. N., Jr *Int. J. Chem. Kinet.* **1983**, *15*, 619.
(111) Oh, S.; Andino, J. M. *Int. J. Chem. Kinet.* **2001**, *33*, 422.
(112) Sorensen, M.; Kaiser, E. W.; Hurley, M. D.; Wallington, T. J.; Nielsen, O. J. *Int. J. Chem. Kinet.* **2003**, *35*, 191.
(113) Srinivasan, N. K.; Su, M. C.; Michael, J. V. *J. Phys. Chem. A* **2007**, *111*, 3951.
(114) Atkinson, R.; Baulch, D. L.; Cox, R. A.; Crowley, J. N.; Hampson, R. F., Jr.; Hynes, R. G.; Jenkin, M. E.; Kerr, J. A.; Rossi, M. J.; Troe, J. Data Sheet HOx_VOC23. In I; IUPAC Subcommittee on Gas Kinetic Data Evaluation for Atmospheric Chemistry; August 2007, *Vol. Web Version*.
(115) Dobe, S.; Berces, T.; Temps, F.; Wagner, H. G.; Ziemer, H. *25th Symposium (International) on Combustion, [Proceedings]*; 1994, 775.
(116) Schatz, G. C. *J. Phys. Chem.* **1995**, *99*, 7522.
(117) Capecehi, G.; Werner, H. J. *Phys. Chem. Chem. Phys.* **2004**, *6*, 4975.
(118) Manthe, U.; Capecchi, G.; Werner, H. J. *Phys. Chem. Chem. Phys.* **2004**, *6*, 5026.
(119) Florian, J.; Leszczynski, J.; Johnson, B. G.; Goodman, L. *Mol. Phys.* **1997**, *91*, 439.
(120) Hoper, U.; Botschwina, P.; Koppel, H. *J. Chem. Phys.* **2000**, *112*, 4132.
(121) Schmidt-Klugmann, J.; Koppel, H.; Schmatz, S.; Botschwina, P. *Chem. Phys. Lett.* **2003**, *369*, 21.
(122) Marenich, A. V.; Boggs, J. E *J. Chem. Phys.* **2005**, *122*, 024308–1.
(123) Barckholtz, T. A.; Miller, T. A. *Int. Rev. Phys. Chem.* **1998**, *17*, 435.
(124) Feilberg, K. L.; Griffith, D. W. T.; Johnson, M. S.; Nielsen, C. J. *Int. J. Chem. Kinet.* **2005**, *37*, 110.
(125) Joseph, T.; Steckler, R.; Truhlar, D. G. *J. Chem. Phys.* **1987**, *87*, 7036.
(126) Corchado, J. C.; Truhlar, D. G.; Espinosa-Garcia, J. *J. Chem. Phys.* **2000**, *112*, 9375.
(127) Skodje, R. T.; Truhlar, D. G.; Garrett, B. C. *J. Phys. Chem.* **1981**, *85*, 3019.
(128) Saueressig, G.; Crowley, J. N.; Bergamaschi, P.; Bruhl, C.; Brenninkmeijer, C. A. M.; Fischer, H. *J. Geophys. Res. [Atmospheres]* **2001**, *106*, 23127.
(129) Gierczak, T.; Talukdar, R. K.; Herndon, S.; Vaghjiani, G. L.; Ravishankara, A. R. *J. Phys. Chem. A* **1997**, *101*, 3125.
(130) Gola, A. A.; D′Anna, B.; Feilberg, K. L.; Sellevaag, S. R.; Bache-Andreassen, L.; Nielsen, C. J. *Atmos. Chem. Phys.* **2005**, *5*, 2395.
(131) Sellevåg, S. R.; Nyman, G.; Nielsen, C. J. *J. Phys. Chem. A* **2006**, *110*, 141.

JP805643X